Published in final edited form as:
Brain Cell Biol. 2006 December ; 35(4-6): 207–228. doi:10.1007/s11068-008-9019-6.

Imaging Synaptic Inhibition in Transgenic Mice Expressing the Chloride Indicator, Clomeleon

K. Berglund[1], **W. Schleich**[2], **P. Krieger**[2], **L.S. Loo**[1], **D. Wang**[1], **N.B. Cant**[1], **G. Feng**[1], **G.J. Augustine**[1,#], and **T. Kuner**[2,#]

1 *Dept. of Neurobiology, Duke Univ. Medical Center, Box 3209, Durham, NC 27710*

2 *Dept. of Cell Physiology, Max Planck Institute for Medical Research, Jahnstrasse 29, 69120 Heidelberg, Germany*

Abstract

We describe here a molecular genetic approach for imaging synaptic inhibition. The thy-1 promoter was used to express high levels of Clomeleon, a ratiometric fluorescent indicator for chloride ions, in discrete populations of neurons in the brains of transgenic mice. Clomeleon was functional after chronic expression and provided non-invasive readouts of intracellular chloride concentration ($[Cl^-]_i$) in brain slices, allowing us to quantify age-dependent declines in resting $[Cl^-]_i$ during neuronal development. Activation of hippocampal interneurons caused $[Cl^-]_i$ to rise transiently in individual postsynaptic pyramidal neurons. $[Cl^-]_i$ increased in direct proportion to the amount of inhibitory transmission, with peak changes as large as 4 mM. Integrating responses over populations of pyramidal neurons allowed sensitive detection of synaptic inhibition. Thus, Clomeleon imaging permits non-invasive, spatiotemporally resolved recordings of $[Cl^-]_i$ in a large variety of neurons, opening up new opportunities for imaging synaptic inhibition and other forms of chloride signaling.

Keywords

chloride regulation; chloride imaging; GABA receptors; inhibitory synaptic transmission; interneuron

Introduction

Imaging is the most practical means of determining the activity patterns of neural circuits in the brain. Voltage-sensitive dyes, Ca^{2+} indicators, intrinsic signal imaging and fMRI, have been used to image neural activity over dimensions ranging from individual synapses to large populations of neurons (Mao et al., 2001; Mrsic-Flogel et al., 2003; Grinvald and Hildesheim, 2004; Baker et al., 2005). However, the signals employed by these methods mainly rely on neuronal excitation. Apart from a few reports of successful imaging of inhibitory circuit activity though the use of voltage-sensitive dyes (Horikawa et al., 1996; Cohen and Yarom, 2000; Derdikman et al., 2003), autofluorescence (Ebner et al., 2005), pH indicators (Elias et al., 1993) and organic Cl^- indicator dyes (Isomura et al., 2003), synaptic inhibition has largely remained invisible even though inhibition contributes fundamentally to neuronal computation.

#Corresponding authors: Thomas Kuner, Current address: Institute of Anatomy and Cell Biology, University of Heidelberg, Im Neuenheimer Feld 307, 69120 Heidelberg, Germany, Tel +49 6221 548678, Fax +49 6221 544952, Email: E-mail: kuner@uni-heidelberg.de. George Augustine, Phone: +1 919 681 6164, Fax: +1 919 681 9866, Email: E-mail: georgea@neuro.duke.edu.

Fast synaptic inhibition is mainly mediated by Cl^- fluxes. Depending on the intracellular chloride concentration ($[Cl^-]_i$) and the membrane potential, Cl^- fluxes through ionotropic γ-aminobutyric acid (GABA) and glycine receptors can either hyperpolarize or depolarize the membrane (Kaila, 1994). Furthermore, Cl^- conductances can shunt concomitant fluxes of cations without affecting membrane potential, making such forms of inhibition virtually invisible to voltage recordings. However, all of these inhibitory actions result from Cl^- fluxes that will yield changes in postsynaptic $[Cl^-]_i$ (Kaila, 1994; Kuner and Augustine, 2000; Marandi et al., 2002; Isomura et al., 2003; Jedlička and Backus, 2006). Thus, direct measurements of changes in $[Cl^-]_i$ seem an ideal means of imaging synaptic inhibition.

Clomeleon is a genetically-encoded indicator that permits optical determination of resting $[Cl^-]_i$ in the physiologically relevant range and visualization of Cl^- transients elicited by activation of GABA receptors (Kuner and Augustine, 2000). Unlike organic Cl^- dyes (Verkman, 1990), Clomeleon expression can be targeted to distinct populations of neurons. These properties make Clomeleon suitable for studying many poorly understood aspects of $[Cl^-]_i$ regulation, including activity-dependent ionic plasticity (Kaila, 1994; Payne et al., 2003), compartmental gradients of $[Cl^-]_i$ (Duebel et al., 2006; Szabadics et al., 2006), sensory signal transduction (Reuter et al., 1998), and pathophysiological mechanisms in a multitude of diseases (Payne et al., 2003; Pond et al., 2006).

Here we consider the use of Clomeleon for imaging Cl^--mediated synaptic inhibition in neuronal networks. Such an approach holds promise for revealing the spatiotemporal patterns of synaptic inhibition in neuronal populations during inhibitory circuit activity, yielding fundamental insights into the function of neuronal networks. To achieve this goal, we have developed a set of indicator mouse lines expressing Clomeleon under the control of the thy1 promoter (Feng et al., 2000), giving rise to Clomeleon expression in different neuronal subsets. We first describe the patterns of Clomeleon expression in these mouse lines and show that this indicator functions normally after chronic expression. Measurements of $[Cl^-]_i$ with Clomeleon demonstrate that resting $[Cl^-]_i$ differs between neurons and decreases during postnatal maturation. Finally, we show that activation of inhibitory synapses produces a detectable, transient increase in $[Cl^-]_i$ that is proportional to the amount of synaptic inhibition, thereby providing a means of quantifying inhibition in space and in time. Thus, Clomeleon indicator mouse lines provide powerful tools for measuring $[Cl^-]_i$ in neurons and, thereby, for visualizing inhibitory circuit activity.

Results

Expression of Clomeleon in brain of transgenic mice

Clomeleon cDNA was cloned into the mouse *thy1.2* vector (Fig. 1a) and this targeting vector was used to create transgenic mice (see Methods section). Out of 9 transgenic founders, 6 lines expressing Clomeleon in different regions of the brain were recovered and designated as CLM lines. Thy1-driven transgenic expression can vary with respect to the brain region, number of neurons per region, concentration of Clomeleon per cell, and the temporal expression profile in postnatal life (Feng et al., 2000). To identify the pattern of Clomeleon expression within the CLM1 line, a series of sagittal sections were cut from one hemisphere of a paraformaldehyde-fixed brain of an adult CLM1 mouse (Fig. 1b). In this line, robust expression of Clomeleon was observed in cerebellar granule cells, dentate gyrus granule cells and CA1 neurons of the hippocampus, principal cells in the amygdala, the nucleus of the lateral olfactory tract, the mammilary nucleus, the pontine nuclei and many other brain regions.

Thy1-driven variations were observed when comparing the expression of Clomeleon in different lines of transgenic mice (Figs. 2a–c). Within neuronal subsets, Clomeleon expression ranged from low to very strong. The patterns of expression in all of the Clomeleon transgenic

mice are summarized in Table 1. Most lines showed robust expression of Clomeleon in hippocampal CA1 pyramidal neurons and dentate gyrus granule cells, mossy fiber terminals of the cerebellum and their somata in the pontine nucleus, brainstem nuclei, thalamic neurons, neurons located in glomeruli of the olfactory bulb (Figs. 2a–c) and retinal neurons (Haverkamp et al., 2005). Regional differences included expression in mitral cells of the olfactory bulb (CLM1, 2 and 12), cortical pyramidal neurons of layer 2/3 (Fig. 2d) and layer 5 (CLM1, 11 to 13; Figs. 2e, f), several types of neurons in the hippocampus (Figs. 2g–i), and neurons in the amygdala, thalamus, basal ganglia, and other regions (Table 1; see also Fig. 1b). The number of neurons expressing Clomeleon in any given area ranged from low density ("+" in Table 1), e.g. in the cortex of CLM13, to a very high density ("+++" in Table 1) of expression in the CA1 of CLM11, dentate gyrus in CLM13, and inferior colliculus in CLM12 (Figs. 2a–i). However, no line was recovered with a sparse, Golgi-type of expression as reported when using the thy-1 promoter to express other GFP derivatives in mice (Feng et al., 2000). The expression patterns described here were stably transmitted over several generations in all of the lines generated.

Weak thy-1-directed Clomeleon expression could be detected as early as postnatal day 2 (P2) in CLM11, with most other lines showing expression at P8 and maximal levels after P14. Clomeleon fluorescence was evenly distributed in all compartments of expressing neurons (Fig. 2), suggesting that readouts of $[Cl^-]_i$ should not be biased by clustering or segregation into subcellular compartments. In summary, robust Clomeleon expression suitable for optical imaging could be detected in different neuronal subsets from early postnatal stages onwards.

Long-term effects of Clomeleon expression

Long-term expression of GFP and genetically encoded indicators derived from it could lead to degradation by proteases. Proteolytic cleavage of Clomeleon would destroy its functionality, because the FRET-mediated readout of $[Cl^-]$ depends on the close spatial proximity and 1:1 stoichiometry ratio of the Cl^--sensitive YFP and the insensitive CFP. To examine the possibility of proteolytic cleavage of Clomeleon, we used an anti-GFP antibody to probe for the presence of Clomeleon protein in brain lysates of Clomeleon mice at the age of 3 weeks and 9 months. SDS-PAGE analysis showed that proteolytic cleavage was virtually undetectable in Clomeleon from brain samples of both young and old mice (Fig. 3a).

Chronic expression of Clomeleon also could cause cellular toxicity. However, it is unlikely that chronic Clomeleon expression is toxic, because CLM mice lived for 2 years or longer without any noticeable behavioral deficits. To consider the possible effects of Clomeleon expression on the physiological properties of neurons, patch-clamp recordings were made from Clomeleon-expressing neurons in cortical slices from CLM1 and CLM11 mice (age P14–28). These recordings (Fig. 3b) revealed the two known types of layer 5 pyramidal neurons, bursting and regular firing (Agmon and Connors, 1992). Clomeleon-expressing neurons exhibited normal electrophysiological properties when compared to neurons from wildtype mice at P20 (Table 2, ANOVA, $p > 0.05$), suggesting that they were not compromised by long-term expression of Clomeleon.

In summary, we conclude that Clomeleon can be expressed chronically in transgenic mice without causing cellular toxicity or any other obvious defects in Clomeleon-expressing neurons. Thus, our efforts yielded a set of transgenic mouse lines with patterns of Clomeleon expression that should allow quantitative Cl^- imaging in many different types of neurons.

Clomeleon reports resting $[Cl^-]_i$

We first tested the functionality of Clomeleon by examining its sensitivity to Cl^-. For this purpose, we examined Clomeleon properties in cultured primary hippocampal neurons and in

acute brain slices prepared from CLM mice. In the cultured neurons, Cl^- titration curves were established by equilibrating intracellular Cl^- with that of the patch pipette (Fig. 4a, open circles), as in Kuner and Augustine (2000), or by using the ionophores nigericin and tributyltin to equilibrate $[Cl^-]_i$ with extracellular $[Cl^-]$ (Fig. 4a, filled circles), as in Pond et al. (2006). In both cases, the ratio of Clomeleon fluorescence emission varied with $[Cl^-]_i$ and the two methods of manipulating $[Cl^-]_i$ yielded very similar titration curves. Furthermore, the ionophore method yielded very similar results in brain slices (Fig. 4a, red squares). For each value of $[Cl^-]_i$, the data points obtained in these 3 conditions were indistinguishable (ANOVA, $p > 0.05$). These results demonstrate that Clomeleon is fully functional in mice after chronic expression.

Such calibration of Clomeleon then allowed us to determine resting $[Cl^-]_i$ in different types of neurons. To ensure reliable determination of absolute $[Cl^-]_i$, images were obtained under conditions that minimized photobleaching (see Methods section). Resting $[Cl^-]_i$ was measured in hippocampal CA1 neurons, cortical layer 5 neurons, amygdalar neurons and cerebellar granule cells in slices obtained from adult (>P20) mice from various CLM lines. Fig. 4b illustrates imaging of resting $[Cl^-]_i$ in CA1 neurons. The fluorescence signal generated by FRET-mediated excitation of YFP showed an excellent signal to background ratio of 20–100 (Fig. 4b, left), whereas emission of the CFP donor was less intense, being 10–50 times brighter than the background (Fig. 4b, center). Because ratios are very sensitive to the quantity in the denominator, special care was taken to minimize errors linked to measurement of the relatively dim CFP signals (see Methods section).

Measurement of resting $[Cl^-]_i$ in slices from several regions of P21 mouse brain revealed that hippocampal CA1 neurons, cortical neurons, amygdalar pyramidal cells and cerebellar granule cells had comparably low values of $[Cl^-]_i$ (Fig. 4c). This condition permits hyperpolarizing inhibitory signaling, via inward Cl^- currents, which is required for proper network function. Typically, the somata of the CA1 neurons (age P21) revealed a low $[Cl^-]_i$ (Fig. 4b, right), with a mean value of 6.6 ± 0.4 mM (mean ± SEM; n = 69). There was a tendency towards higher $[Cl^-]_i$ in the stratum radiatum, where the dendrites of CA1 pyramidal cells are the only structures expressing Clomeleon, suggesting that $[Cl^-]_i$ may be higher in the dendrites of these cells than in their cell bodies (see below). In all slices examined, the layer of neurons at the surface of the slice invariably showed cells with $[Cl^-]_i$ approaching extracellular concentrations, consistent with the common observation that superficial cells are damaged during the slicing procedure.

A switch in GABAergic transmission, from depolarization to hyperpolarization, during neuronal development has been demonstrated in many studies (Ben-Ari et al., 1989; Cherubini et al., 1991; Owens et al., 1996). Although this presumably is due to a progressive drop in $[Cl^-]_i$, direct measurement of $[Cl^-]_i$ at different postnatal stages has not yet been possible in slices. We therefore determined $[Cl^-]_i$ in cortical and CA1 pyramidal neurons at different ages. For this purpose, we used the CLM11 line, which expresses Clomeleon in cortical neurons from age P2 onwards. $[Cl^-]_i$ in these neurons could reliably be determined at P5 and later (Fig. 5a). At P5, $[Cl^-]_i$ varied widely between cells; the distribution of $[Cl^-]_i$ suggested at least two populations of neurons, a main population with a $[Cl^-]_i$ of about 20 mM and a smaller population with $[Cl^-]_i$ of approximately 30 mM (Fig. 5b, top). An additional group of neurons with a $[Cl^-]_i$ around 10 mM might have also been present. These observations parallel previous results in cultured hippocampal neurons (Kuner and Augustine, 2000). At older ages, the distributions of $[Cl^-]_i$ became narrower, suggesting a more homogenous population of neurons at more mature stages (Fig. 5b). Mean $[Cl^-]_i$ decreased over development, dropping from 21.5 ± 0.7 mM (mean ± SEM, n = 115) at P5 to 5.5 ± 0.5 mM (n = 80) at P20.

The developmental progression of $[Cl^-]_i$ is summarized in Fig. 5c. This relationship indicates that low $[Cl^-]_i$ was reached at the end of the third postnatal week, consistent with the functional changes in polarity of GABAergic responses and the expression profiles of KCC2 and NKCC1 transporters (Rivera et al., 1999;Stein et al., 2004). The Cl^- equilibrium potential, E_{Cl}, calculated from these measurements hyperpolarized by more than 30 mV between P5 and P20 (Fig. 5d). In conclusion, the $[Cl^-]_i$ described here on the basis of non-invasive optical imaging supports the hypothesis that postnatal changes in the Cl^- electrochemical gradient underlies the functional switch in GABAergic transmission during development.

Clomeleon detects Cl^- changes due to inhibitory synaptic activity

After establishing that Clomeleon can record steady-state $[Cl^-]_i$ in targeted neurons, we next examined whether Clomeleon can report dynamic changes in $[Cl^-]_i$ associated with activation of inhibitory synapses. We imaged $[Cl^-]_I$ in hippocampal slices prepared from the CLM1 line, where most CA1 pyramidal cells expressed Clomeleon robustly (Fig. 1b; see also Pond et al., 2006). To stimulate the GABAergic interneurons that form inhibitory synapses with CA1 pyramidal neurons, we placed an extracellular electrode at the distal part of the apical dendrites (Freund and Buzsáki, 1996;Somogyi and Klausberger, 2005). A glutamate receptor antagonist, kynurenic acid (2–3 mM), was routinely added to the extracellular solution to suppress excitatory synaptic transmission.

In the first series of experiments, whole-cell patch clamp recordings were obtained from individual Clomeleon-positive CA1 neurons. This allowed us to control the driving force on Cl^- fluxes and also to monitor inhibitory postsynaptic currents (IPSCs). A pyramidal cell was voltage-clamped at a potential of −45 mV and $[Cl^-]_i$ was set to 5 mM to obtain outward IPSCs in response to brief electrical stimuli. The number of inhibitory synapses that are activated by such stimuli will depend on the intensity of the stimulus. To estimate the number of interneurons that were activated by the stimuli that we employed, we recorded IPSCs evoked by single stimuli of variable intensity (Fig. 6a). Under our conditions, a single stimulus evoked IPSCs 50–150 pA in amplitude, with the relationship between mean IPSCs amplitude and stimulus intensity shown in Fig. 6b. IPSCs increased in proportion to stimulus intensity with a slope of 90 pA/mA (n = 7). To calculate the number of interneurons activated by the stimuli, the published value for the mean amplitude of unitary IPSCs (26 pA) produced at the synapse between an identified GABAergic oriens-lacunosum moleculare interneuron and a pyramidal cell in rat hippocampal slices (Maccaferri et al., 2000) was adjusted to account for the different driving force on Cl^- in our recording conditions. Thus, the relationship of Fig. 6b has a slope of 6 interneurons/mA, meaning that approximately 3–10 interneurons were activated per pyramidal cell with the range of stimulus intensities that we used (400 μA–1.5 mA).

Single stimuli within this range did not produce measurable changes in Clomeleon fluorescence. However, a train of such stimuli evoked summating IPSCs (Fig. 7a, top) that caused a transient reduction in the fluorescence of the YFP acceptor and a concomitant increase in the fluorescence of the CFP donor of Clomeleon simultaneously recorded from the soma of the same cell (Fig. 7a, center). Such fluorescence changes could then be converted into changes in $[Cl^-]_i$ (Fig. 7a, bottom). The rise in $[Cl^-]_i$ lagged behind the current response by about one second, presumably due to both the time required for Cl^- accumulation in the cell body and the response time of Clomeleon (Kuner and Augustine, 2000). The rise in $[Cl^-]_i$ persisted for much longer than the current, indicating slow removal of Cl^- from the cell. In this experiment, both IPSCs and the rise in $[Cl^-]_i$ were completely blocked by the $GABA_A$ receptor antagonist SR95531 (SR; Fig. 7b, center), demonstrating that both were mediated by $GABA_A$ receptors. After washout of the antagonist (Fig. 7b, right), both responses recovered partially, with residual block most likely due to incomplete removal of SR from the slice. While IPSCs were blocked almost completely by SR in every experiment, stimulus-induced rises in $[Cl^-]_i$ were

blocked in 9 out of 14 experiments. Responses not blocked by SR presumably were caused by the $GABA_A$-receptor independent component of synaptic Cl^- influx reported by (Isomura et al., 2003). Only responses that clearly were blocked by SR were used for subsequent analysis.

To determine the sensitivity of Clomeleon to Cl^- fluxes associated with synaptic inhibition, the number of IPSCs was varied by changing the duration of the stimulus train. We found a saturating relationship between the number of stimuli applied and the resulting $[Cl^-]_i$ changes (Fig. 7c). This relationship could be described by the Michaelis-Menten equation (continuous curve in Fig. 7c), with a maximum $[Cl^-]_i$ change of 9.5 mM and half-maximal response at 150 stimuli. Fig. 7d shows the relationship between Cl^- influx, measured as the integral of IPSCs, and the magnitude of the resultant changes in somatic $[Cl^-]_i$ reported by Clomeleon. There was a linear relationship between Cl^- influx and $[Cl^-]_i$, with a correlation coefficient of 0.98 ($p < 0.0001$, Pearson test, $n = 11$). This indicates that Clomeleon quantitatively reports the Cl^- fluxes associated with synaptic inhibition. The slope of the relationship shown in Fig. 7d was 8 μM/pC, though this value may be an underestimate because of possible contributions of out-of-focus fluorescence from other, unclamped neurons. The shaded area shown in Figs. 7c and d indicates the recording noise level, determined as the root mean square (RMS) value of resting $[Cl^-]_i$. Under the conditions of Fig. 7, this noise level was 0.8 ± 0.2 mM (mean ± SEM, $n = 6$). Given the relationships shown in Figs. 7c and d, this is equivalent to approximately 15 IPSCs or 100 pC of Cl^- influx. However, signal averaging across repeated trials significantly improved this signal-to-noise ratio (SNR). For example, the $[Cl^-]_i$ traces shown in Fig. 7a represent averages of 3 consecutive identical trials. This reduced the basal fluctuations in $[Cl^-]_i$ by approximately 50%, very close to the theoretical prediction that the SNR should be increased in proportion to the square root of the number of trials, i.e. by $3^{1/2}$. With such signal averaging, the noise was lowered to the equivalent of 68 pC of Cl^- flux or 9 IPSCs. The square-root improvement in SNR means that detection of responses to single IPSCs would require averaging approximately 15^2, or 225, trials. In summary, our results indicate that Clomeleon can detect changes in $[Cl^-]_i$ in the somata of single voltage-clamped neurons following brief trains of IPSCs.

Clomeleon detects Cl^- changes in unperturbed neurons

Unlike the situation when recording IPSCs under voltage-clamp conditions, the changes in membrane potential produced by inhibitory postsynaptic potentials (IPSPs) will cause the driving force on Cl^- influx to decline during the IPSP, thereby reducing Cl^- flux. Because this effect could limit the ability to image inhibitory transmission, we next asked whether Clomeleon could image inhibitory synaptic transmission in hippocampal neurons that were not voltage-clamped.

For this purpose, we measured $[Cl^-]_i$ optically while using whole-cell current clamp recordings from a pyramidal cell to simultaneously measure IPSPs (Fig. 8a). Under our conditions, an IPSP produced by a single stimulus caused a 5.1 ± 1.0 mV hyperpolarization from the resting membrane potential of −70.8 ± 1.9 mV (mean ± SEM, $n = 6$). Trains of stimuli evoked IPSPs that typically peaked in amplitude during the third or fourth stimulus in the train and then depressed (Fig. 8b). Simultaneous Clomeleon imaging revealed barely detectable changes in $[Cl^-]_i$ in the soma of the same cell (Fig. 8c). To improve the SNR, $[Cl^-]_i$ signals were collected from many somata in the pyramidal cell layer. For this purpose, we measured fluorescence from an area that covered the entire stratum pyramidale in a given field and typically contained 10–20 fluorescent somata (Fig. 8a). Our assumption was that the population of cells should have IPSPs similar to those of the cell where IPSPs were being measured, allowing integration over a larger number of Clomeleon molecules. This strategy improved the SNR significantly, so that responses to brief trains of IPSPs were readily detected (Fig. 8d). When the duration of the stimulus train was varied, $[Cl^-]_i$ increased in a saturable fashion, with a maximum $[Cl^-]_i$

change of 1.8 mM and half-maximal response at 45 stimuli (Fig. 8e). These parameters both are smaller than those obtained from voltage clamp experiments (Fig. 7c), consistent with our expectation that the Cl^- driving force in unclamped cells is reduced during synaptic activity.

Saturation of Clomeleon responses presumably is due to several factors that depress IPSPs during the train (Fig. 8b), such as the reduction in Cl^- driving force, depression of GABA release, and/or desensitization of $GABA_A$ receptors. To take into account such time-dependent changes in IPSPs, we calculated the time integral of IPSPs and found that the $[Cl^-]_i$ changes were proportional ($r = 0.99$; $p < 0.02$, Pearson test) to the IPSP integral (Fig. 8f). Thus, the Clomeleon signals accurately reflect the amount of inhibitory synaptic transmission in neurons that were not voltage clamped. Measuring $[Cl^-]_i$ over many cells reduced the noise level to approximately 170 ± 40 μM (mean ± SEM, n = 4), shown by the shaded area in Fig. 8f, corresponding to a detection threshold of only 5 IPSPs. Averaging over 4 trials further improved the noise level by approximately 47%, reducing the detection limit to 90 μM or approximately 3 IPSPs.

The experiments above demonstrate that Clomeleon transgenic mice enable $[Cl^-]_i$ imaging of inhibitory transmission. The responses reported by Clomeleon are directly proportional to the amount of inhibitory synaptic activity and require no manipulation of the Cl^- driving force. This opens up the possibility of visualizing synaptic inhibition in physiological conditions without any recording electrodes. To further evaluate this capability, we used Clomeleon imaging to examine the spatial properties of inhibitory responses produced in pyramidal cells. For this purpose, interneurons were stimulated as above and the resulting changes in pyramidal cell $[Cl^-]_i$ were measured using a low magnification objective lens (10x) to observe all layers of area CA1.

Under these conditions, Clomeleon could detect increases in $[Cl^-]_i$ in all layers of area CA1 following activation of inhibitory synapses and allowed us to detect recruitment of presynaptic interneurons with increasing stimulus intensity (Fig. 9). At the minimal stimulus intensity tested (200 μA), no consistent response was detected (Fig. 9a). However, a 400 μA stimulus elicited a response in apical dendrites, near the tip of the stimulating electrode (Fig. 9b). Stronger stimuli caused $[Cl^-]_i$ changes that extended to the somata and basal dendrites of the CA1 pyramidal cells (Figs. 9c and d), Fig. 9e quantify the averaged $[Cl^-]_i$ changes from the whole CA1 in the field, recorded in a total of 4 experiments. The magnitude of the $[Cl^-]_i$ change was proportional to stimulus intensity and was blocked by SR, indicating that the $[Cl^-]_i$ changes resulted from progressive activation of GABAergic neurons by stronger stimuli. In addition, these responses showed no signs of saturation, indicating that not all inhibitory synapses were activated by the maximal stimulus (1.5 mA). This is consistent with observations that IPSCs increased in proportion to the intensity of these stimuli (Fig. 6b).

The temporal and spatial characteristics of the changes in $[Cl^-]_i$ resulting from inhibitory activity were characterized in detail in experiments where the number of stimuli were varied. Similar to the results shown in Fig. 8, $[Cl^-]_i$ increased in proportion to the number of stimuli (Figs. 10a–d). By integrating over the entire area of activity, we could observe that the time course was independent of the number of stimuli: in all cases, responses reached a peak soon after the end of the IPSP train and decayed over the next 30–60 s (Fig. 10e). The peak amplitude of these responses was somewhat larger than for the responses analyzed in Fig. 8e, with a maximum $[Cl^-]_i$ change of 3.1 mM predicted from Michaelis-Menten fits (data not shown). This difference is due to the fact that these signals were dominated by dendritic responses, which are larger than the somatic responses analyzed in Fig. 8 (see below).

To explore the origins of these responses, we first examined their sensitivity to SR. This drug very effectively eliminated these responses, reducing them by 87 ± 2% (mean ± SEM, n = 7).

We next examined their sensitivity to external Ca^{2+}, which is required for synaptic release of GABA (Duarte et al., 1993). Ca^{2+} removal reversibly blocked the stimulus-evoked changes in $[Cl^-]_i$ in all 6 slices tested (Fig. 10f). Thus, the responses result from Clomeleon detecting the actions of GABA that is released from interneurons and activates $GABA_A$ receptors on postsynaptic pyramidal cells.

The images in Figs. 10a–d reveal spatial heterogeneity in the $[Cl^-]_i$ changes produced by inhibitory synaptic activity. To characterize the spatial dynamics of these Cl^- responses, we generated line scans displaying the magnitude of $[Cl^-]_i$ changes as a function of space and time. Because Clomeleon was expressed only in the CA1 neurons, we could be confident that the responses were generated exclusively in these cells. The area of analysis covered several layers within the CA1 region, including the stratum lacunosum-moleculare (comprising the distal parts of pyramidal cell apical dendrites), the stratum radiatum (the proximal parts of apical dendrites), the stratum pyramidale (somata) and the stratum oriens (basal dendrites). Resting $[Cl^-]_i$ in each compartment was similar: 5.7 ± 1.6 mM in distal apical dendrites; 10.3 ± 3.2 mM in proximal apical dendrites; 5.0 ± 4.8 mM in somata; 8.0 ± 3.7 mM in the basal dendrites (mean ± SEM, n = 7). Though there was a tendency for resting $[Cl^-]_i$ to be higher in dendrites than in somata, this difference was not significant (ANOVA, $p > 0.5$).

Fig. 11a presents an analysis of the spatiotemporal properties of responses within the region shown by the white rectangle in Fig. 10d. In this figure, resting $[Cl^-]_i$ before stimulation was subtracted to obtain relative changes in $[Cl^-]_i$ caused by stimulation. $[Cl^-]_i$ changes in the CA1 neurons were largest in apical dendrites, the location closest to the site of stimulation, and were smaller elsewhere. The time course of these changes varied somewhat across compartments, as can be seen most clearly when $[Cl^-]_i$ changes were averaged in each region (Fig. 11b). While $[Cl^-]_i$ changes in the distal part of apical dendrites rose rapidly and reached a maximum at the end of the train of stimuli, $[Cl^-]_i$ rose more slowly in basal dendrites and in the proximal part of apical dendrites (Fig. 11b). The $[Cl^-]_i$ rise was slowest in somata, probably due to slow diffusion of Cl^- from the dendrites and/or from the surface membrane of the somata.

A summary of the analyses on the peak amplitude and the time to peak for 7 experiments is shown in Figs. 11c and d. These analyses emphasize that the $[Cl^-]_i$ changes were large and fast in the apical dendrites and were smaller and slower in the somata and basal dendrites of the CA1 pyramidal cells. These differences presumably reflect differences in the location of active inhibitory synapses, in the surface-to-volume ratio of the different compartments and in the driving force on Cl^- (Staley and Proctor, 1999).

In summary, these results document that Clomeleon can detect changes in postsynaptic $[Cl^-]_i$ resulting from synaptic GABA receptor activation, thereby establishing the utility of Clomeleon transgenic mice for imaging synaptic inhibition in the brain.

Discussion

This paper characterizes a set of indicator mouse lines uniquely suited to non-invasive determinations of $[Cl^-]_i$ in neurons. Although these mice have previously been used for several purposes (Haverkamp et al., 2005; Duebel et al., 2006; Pond et al., 2006), this paper provides the first comprehensive description of these mice and the properties of the transgenically expressed Clomeleon. We also demonstrate that dynamic changes in $[Cl^-]_i$ resulting from synaptic activity can be detected in these mice, establishing a new avenue for imaging mechanisms of synaptic inhibition and inhibitory network activity.

Functional integrity of Clomeleon after chronic overexpression

Given the limited success of expressing genetically encoded probes, especially Ca^{2+}-sensing indicators, in transgenic mice (Hasan et al., 2004; Reiff et al., 2005), we carefully examined the functionality of chronically expressed Clomeleon protein (Figs. 3 and 4). Several observations point to the conclusion that Clomeleon functions well even after chronic expression. First, calibration experiments using the ionophores tributyltin and nigericin in brain slices prepared from CLM lines yielded titration curves identical to those obtained from cultured neurons, suggesting that Clomeleon is fully sensitive to $[Cl^-]_i$ (Fig. 4a). Second, Clomeleon was not cleaved proteolytically, even after chronic expression for 9 months (Fig. 3a). This is important because accurate readout of $[Cl^-]_i$ by Clomeleon depends on a 1:1 stoichiometry of CFP to YFP, as well as close spatial proximity of these two fluorophores (Kuner and Augustine, 2000). Third, the electrophysiological properties of neurons expressing Clomeleon were normal, suggesting that Clomeleon is not toxic (Fig. 3b). Furthermore, animals survived for up to 2 years without showing any obvious abnormalities. In summary, these observations demonstrate that Clomeleon protein can be chronically expressed in mice without impairing the function of the indicator or the mouse.

Measuring $[Cl^-]$ with Clomeleon

The high levels of Clomeleon expressed under the control of the thy1 promoter provide an excellent basis for quantitative $[Cl^-]$ imaging. In confocal imaging, the signal often exceeded the background by a factor of 50 in the YFP channel and 25 in the CFP channel. When imaged with a wide-field microscope, the signal/background ratio was typically larger than 65. The YFP:CFP ratio emission ratio of Clomeleon decreases by 24% in response to an increase in $[Cl^-]$ from 0 to 50 mM. This compares favorably to the signals reported by Cameleon, a Ca^{2+} indicator, following transgenic expression in mice: synaptic activity causes the FRET ratio of this indicator to change less than 1% (Hasan et al., 2004; Reiff et al., 2005). The sensitivity of Clomeleon is slightly poorer than that of organic Cl^- indicator dyes such as 6-methoxy-*N*-ethylquinolinium chloride (MEQ); the apparent Cl^- dissociation constant in hippocampal CA1 pyramidal cells was 182 mM for Clomeleon and 61 mM for MEQ (Inglefield and Schwartz-Bloom, 1997). However, Clomeleon has many other advantages over MEQ, including genetic targeting and ratiometric measurement of absolute $[Cl^-]$. Although the sensitivity of Clomeleon-based measurements of $[Cl^-]$ suffices to determine resting $[Cl^-]_i$ in the physiological range without saturation, for detecting the small Cl^- transients produced by synaptic activity in adult brains it would be useful to improve the Cl^- binding affinity of Clomeleon. Preliminary mutagenesis studies indicate that small changes in amino acid composition of the YFP moiety can improve the Cl^- binding affinity of Clomeleon by more than 10 fold (J. Casad and G.J. Augustine, unpublished results). The time resolution of Clomeleon-based measurements of $[Cl^-]_i$ permits recordings of events on the time scale of inhibitory postsynaptic responses (Figs. 7–11). The kinetics of Cl^- binding by Clomeleon depends on $[Cl^-]$ and temperature, with time constants ranging from 600 ms in low $[Cl^-]$ at 20 °C to 200 ms at 37 °C (W. Schleich and T. Kuner, unpublished results). In summary, Clomeleon mouse lines allow high-resolution determination of $[Cl^-]$ in the physiologically relevant range of concentrations and time courses.

Clomeleon reports neuronal $[Cl^-]_i$

Depolarizing responses to GABA were first described almost 30 years ago (Barker and Ransom, 1978; Obata et al., 1978; Alger and Nicoll, 1979; Andersen et al., 1980). It was later established that the shift from depolarizing GABA responses in young animals to hyperpolarizing responses in adult animals correlated with changes of the equilibrium potential of Cl^- towards more negative potentials (Cherubini et al., 1991; Owens et al., 1996), with the onset of the expression of Cl^--extruding transporters such as KCC2 (Rivera et al., 1999), and

with a decrease in the expression of Cl^--accumulating transporters such as NKCC1 (Yamada et al., 2004). However, the presumed decrease in $[Cl^-]_i$ occurring during development has not yet been visualized in brain slices or *in vivo*. Here, we demonstrate that $[Cl^-]_i$ decreases from ~ 22 to ~ 8 mM during the second postnatal week, and reaches the adult level of ~ 6 mM at P20 in hippocampal CA1 neurons (Fig. 5). Because Clomeleon is also sensitive to changes in pH_i, a developmental alkalinization could mimic a decrease of $[Cl^-]_i$ in Clomeleon-based measurements. To mimic a change in apparent $[Cl^-]_i$ from 22 to 6 mM, the resting pH would have to increase from 6.7 at P5 to 7.25 at P20. However, a constant pH of about 7.1 from birth to P21 has been reported (Bevensee et al., 1996). Thus, we conclude that our measurements accurately reflect changes in $[Cl^-]_i$ over development.

Both the time course and the magnitude of the developmental decreases in $[Cl^-]_i$ reported by Clomeleon are consistent with previous estimates based on electrophysiological measurements (Owens et al., 1996) and the expression profiles of NKCC1 and KCC2 (Rivera et al., 1999; Stein et al., 2004; Yamada et al., 2004; Rivera et al., 2005). Some of these studies showed a rather large variability, both within a given preparation as well as among different cell types, consistent with our finding of a wide distribution of $[Cl^-]_i$ between individual neurons from young mice (Fig. 5). Heterogeneous $[Cl^-]_i$ among different neurons may reflect a diverse mixture of maturational stages in early postnatal development. Our survey of $[Cl^-]_i$ in neurons in different brain areas confirms that most neurons exhibit a low $[Cl^-]_i$ at P21 of around 4–6 mM (Fig. 4c), consistent with $[Cl^-]_i$ inferred from gramicidin perforated patch recordings (Owens et al., 1996; Yamada et al., 2004). A low $[Cl^-]_i$ in mature neurons is a prerequisite to produce hyperpolarizing inhibition, assuming average resting membrane potentials of −60 to −80 mV. Depending on the resting membrane potential and $[Cl^-]_i$, neurons at the higher end of the $[Cl^-]_i$ distribution (Fig. 5) may produce shunting inhibition in response to GABA. Hence, the distribution of $[Cl^-]_i$ in neurons may contribute to the diversity of postsynaptic responses to GABA (Mody and Pearce, 2004).

Changes in $[Cl^-]_i$ triggered by synaptic activity

To determine whether Clomeleon can detect changes in $[Cl^-]_i$ associated with inhibitory synaptic transmission, we first measured $[Cl^-]_i$ in voltage-clamped CA1 neurons during repetitive activation of inhibitory synapses. Clomeleon allowed us to detect the changes in $[Cl^-]_i$ resulting from such activity and to quantify these changes, which ranged from 0.5 to 4 mM. Qualitatively similar responses were detected previously with an organic indicator dye, but the magnitude of the changes in $[Cl^-]_i$ could not be determined because this dye is non-ratiometric (Isomura et al., 2003). Simultaneous patch-clamp recordings revealed that the changes in $[Cl^-]_i$ measured during inhibitory synaptic activity were proportional to the amount of Cl^- flux (Fig. 7d). This result demonstrates that changes in $[Cl^-]_i$, reported by Clomeleon, can be utilized as a direct readout of the amount of inhibitory transmission. Further, our measurements determined that the detection threshold was around 68 pC of Cl^- flux, which was produced by 9 IPSCs under our experimental conditions.

Our results demonstrate – for the first time – that it is possible to image the changes in intracellular Cl^- associated with inhibitory synaptic activity in the absence of any recording electrodes. In physiological conditions, both the membrane potential and the equilibrium potential for Cl^- change in response to Cl^- fluxes. This will eventually neutralize the driving force, limiting the magnitude of changes in $[Cl^-]_i$. Despite this practical challenge, we were able to detect changes in $[Cl^-]_i$ associated with synaptic inhibition in cells that were not voltage clamped. This indicates that voltage clamping is not required to maintain the driving force on Cl^-. The increases in $[Cl^-]_i$ that we measured in CA1 pyramidal cells ranged from 0.25 to 1 mM, which is close to theoretical predictions of these changes (Peter Jedlicka, personal communication). The degree of change in $[Cl^-]_i$ was correlated with the number of stimuli and

with IPSP integral (Figs. 8c and d, respectively), indicating that Clomeleon-based measurements of $[Cl^-]_i$ can be used to infer the amount of inhibitory synaptic activity in a spatiotemporally-defined manner. In neurons that were not voltage-clamped, volume-averaging allowed Clomeleon to resolve increases in $[Cl^-]_i$ of approximately 0.1 mM, resulting from as few as 3 IPSPs. Improvements in the Cl^--binding affinity of Clomeleon should yield better resolution.

These results permit at least two conclusions, one biological and one technological. First, inhibitory synaptic activity causes an accumulation of Cl^- under physiological conditions, resolving a long-lasting debate about whether or not accumulation of Cl^- contributes to synaptic processing (Huguenard and Alger, 1986; Thompson and Gähwiler, 1989; Perkins and Wong, 1997; Isomura et al., 2003; Jedlička and Backus, 2006). Accumulation of postsynaptic Cl^- during synaptic inhibition might contribute to synaptic computation by modifying the driving force on subsequent fluxes of Cl^-, particularly during repetitive activity. Such a form of ionic plasticity could also apply for the reverse case, depletion of intracellular Cl^- (Kuner and Augustine, 2000), which could occur during the depolarizing actions of GABA or glycine in early postnatal stages of maturation. Second, our study provides proof of principle that Clomeleon-based imaging of $[Cl^-]_i$ can be used to visualize inhibitory synaptic activity in neuronal networks. Because of the correlation of changes in $[Cl^-]_i$ and the number of stimuli, readouts of $[Cl^-]_i$ changes could be deconvolved into patterns of inhibitory synaptic activity. Moreover, because Clomeleon is expressed in different types of neurons in the indicator mouse lines introduced here, inhibitory synaptic transmission can be determined in these neuronal subtypes, a powerful feature that is not feasible with other approaches but will be essential for addressing the properties of inhibitory synaptic networks.

Methods

All procedures listed here were approved by the Duke University Animal Care and Use Committee, the guidelines of the Max Planck Society, and the German animal protection act (TierSchG).

Generation of thy1-Clomeleon lines

The DNA fragment encoding Clomeleon was isolated from pQE30-Clomeleon vector (Kuner and Augustine, 2000) using Ecl136II and Bpu1102I and subcloned into the XhoI site of the mouse Thy1.2 vector (Caroni, 1997; Feng et al., 2000) by blunt-end cloning. The thy1.2 vector contains a 6.5 kb genomic fragment from the mouse thy1.2 gene, extending from the promoter to the intron after exon 4 but without the coding region (part of exon 2, entire exon 3 and part of exon 4) and surrounding introns (Fig. 1a). DNA fragments containing the thy1.2 and Clomeleon sequences were isolated with EcoRI and PvuI digestion and gel-purified. Transgenic mice were generated using standard pronuclear injection (Feng et al., 2004). Transgenic founders were identified by PCR from tail DNA with primers in the thy1.2 and Clomeleon sequences (Thy1F1: TCTgAgTggCAAAggACCTTAgg; C24TREV: gTCgTCCTTgAAgAAgATggTgC), which amplify a 550 bp fragment from the transgene. Nine founders were initially identified and backcrossed to C57BL/6 mice to establish transgenic lines. Out of the 9 lines, 6 were found to express Clomeleon in the nervous system.

To characterize the patterns of Clomeleon expression, adult males from several lines were sacrificed with an overdose of halothane and transcardially perfused with 4% paraformaldehyde (PFA) in 0.1 M phosphate buffered saline (PBS, pH 7.4). Brains were removed and stored at 4°C in the fixative overnight. The brains were transferred to cryoprotectant (30%, w/v sucrose in PBS) and then sectioned parasagitally (40 μm thickness). Fluorescence images were obtained with the microscopes described below and photomontages were generated by Photoshop Elements 2.0 (Adobe Systems).

Western blot analysis of Clomeleon expression

Total protein was isolated from two mouse brains at different ages. Defined amounts of protein were loaded on an SDS-PAGE gel and blotted following standard procedures. Bands were visualized with an anti-GFP antibody (1/10000 rabbit GFP antiserum, MoBiTec, Göttingen). For comparison, CFP, YFP and Clomeleon were expressed in bacteria and purified with Nickel affinity chromatography. The N-terminal His-tag and linker added ~2 kD to the molecular mass of the proteins.

Targeted electrophysiological recordings with two-photon laser-scanning microscopy

Patch-clamp recordings from cortical layer 5 neurons expressing Clomeleon were obtained by online overlay of fluorescence and scanning gradient contrast images as described (Wimmer et al., 2004). This method provides a simultaneous display of fluorescence and morphology of the slice with minimal illumination intensities. Membrane potential recordings were corrected for the liquid junction potential (14 mV). Parameters for wild type tissue were taken from (Pérez-Garci et al., 2006) and (Agmon and Connors, 1992).

Determining $[Cl^-]_i$ from FRET ratios

FRET ratios were determined by the ration of CFP/YFP fluorescence emission, as described in Kuner and Augustine (2000). $[Cl^-]_i$ was calculated from the following relationship:

$$[Cl^-]_i = K_d' * [(R_{max} - R)/(R - R_{min})], \quad (1)$$

where R is the measured emission ratio, R_{min} and R_{max} represent the values when Clomeleon is either Cl^- bound or Cl^- free respectively, and K_d' is the effective Cl^- dissociation constant of Clomeleon. As Clomeleon is also pH sensitive, differences in the pH used in calibrations and that measured in situ had to be accounted for. The pH-corrected $[Cl^-]_{corr}$ was calculated according to the relations (1) $K_d^{corr} = 10 \wedge ((0.82 * pH_{corr}) - 3.81)$; (2) $K_d'^{corr} = K_d^{corr} * (K_d'/K_d)$; (3) $R_{meas} = (K_d' * R_{max} + [Cl^-]_{meas} * R_{min})/([Cl^-]_{meas} + K_d')$; (4) $[Cl^-]_{corr} = K_d'^{corr} [(R_{max} - R_{meas})/(R_{meas} - R_{min})]$. K_d was determined from measurements in cuvettes with recombinant Clomeleon protein and was 137 mM (pH = 7.25). K_d' was determined from in situ calibrations.

Two different microscopes were used, in two different countries, to image $[Cl^-]_i$. The details of each system and the experimental procedures used are as follows.

Confocal microscopy—A spinning-disk confocal unit (Visitech) was attached to an upright epifluorescence microscope (DMRXA2, Leica) equipped with a 63x 0.8 NA water immersion objective. An argon ion laser (Coherent) and acusto-optical tunable filter (Visitech) was used for fluorescence excitation at 457 nm. Fluorescence was recorded with two CCD cameras (Sensicam QE, PCO) attached to a divider equipped with a 457/514 nm dichroic mirror and 485-30/535-30 nm emission filters. This arrangement allowed simultaneous recordings of donor and acceptor fluorescence. A third Sensicam QE was mounted on the microscope for infrared DIC imaging. Image-Pro Plus (v4.5.1, Media Cybernetics, Inc.) with a z-stack plugin (v2.4b, Visitech) was used for image acquistion and analysis.

Brain slices were prepared from heterozygous CLM1 and CLM11 mice as described (Wimmer et al., 2004). In brief, the brains were removed from anesthetized and then decapitated animals and placed in a ice-cold solution containing (in mM): 2.5 KCl, 1.25 NaH_2PO_4, 28 $NaHCO_3$, 7 glucose, 1 $CaCl_2$ and 7 $MgCl_2$, 240 sucrose, 1 ascorbate, 3 pyruvate (pH 7.4 after bubbling with 95 % O_2/5 % CO_2, v/v). A custom-built vibratome was used to make 250–350 μm thick coronal sections. Prior to use, slices were incubated at 35°C for 45 min in a solution containing

(in mM): 109 NaCl, 20 HEPES, 25 $NaHCO_3$, 5 KCl, 1.25 NaH_2PO_4, 1.3 $MgCl_2$, 10 glucose and 1.5 $CaCl_2$. For electrophysiological recordings slices were perfused with a saline containing (in mM): 125 NaCl, 2.5 KCl, 1.25 NaH_2PO_4, 1 $MgCl_2$, 25 glucose, 2 $CaCl_2$, 25 $NaHCO_3$, pH 7.4 when bubbled with 95% O_2, 5% CO_2.

As many of the brain regions of interest contained large numbers of neurons expressing Clomeleon, areas of image acquisition were defined in IR-DIC, permitting recordings of fluorescence image stacks without prior wide-field epifluorescence illumination. This approach minimized the risk of differential bleaching of CFP or YFP, which would have resulted in incorrect readouts of $[Cl^-]_I$ (Kuner and Augustine, 2000; Berglund et al., 2005). Confocal excitation intensity was adjusted to keep bleaching minimal (<3% change after 10 s illumination). As the autofluorescence (F_a) cannot be properly defined in CLM mice due to the high fluorescence levels caused by widespread Clomeleon expression, wild type C57B6 mice were used instead. F_a was 3.7±1.8% of the typical YFP fluorescence in the YFP channel and 5.9±3% of the typical CFP fluorescence in the CFP channel. As uncontrolled fluctuations in F_a intensity can cause errors of $[Cl^-]_i$ in the low mM range, the excitation energy was determined before every fluorescence recording with a power meter (Model 840, Newport). A standard F_a curve was determined from different combinations of intensities, exposure times and postnatal age (F_a per pixel per second exposure at 50 μW illumination). The standard curve was used to calculate the background intensity for any imaging condition used. F_a values determined over a period of 1 year were highly stable, justifying the use of the standard curve without frequently repeated measurements. Cyan and Topaz fluorescence were acquired simultaneously, typically from 10–70 μm below the slice surface. Cameras were operated in the 8x8 binning mode with exposure times of 0.2 to 5 s. The ratio CFP and YFP signals corrected for background was determined from ROIs positioned around the somata of individual neurons and converted into $[Cl^-]_i$ according to the calibration shown above. For most recordings, heterozygous mice were used in the experiments. All recordings were done at room temperature.

Calibration—The calibration constants R_{min} = 0.66, R_{max} = 3.85, and K_d' = 133 were determined in primary hippocampal cultures by patching neurons with intracellular solutions containing different concentrations of $[Cl^-]$ (0, 10, 25, 50, 100 mM) or F^- (125 mM) as described previously (Kuner and Augustine, 2000). Electroneutrality was maintained by supplementing appropriate amounts of gluconate. The calibration solution contained (in mM): KCl 10–125, K-gluconate 10–125, NMG-HEDTA 5, HEPES 20 (pH 7.25). Images were acquired 60 to 90 s after break-in, before the whole-cell recording pipette dialyzed too much Clomeleon out of the cell body. Fluorescence intensities were determined from regions of interest (ROIs) drawn around the soma of the neurons.

Wide-field epifluorescence microscopy—An upright epifluorescence microscope (E600-FN, Nikon) was equipped with a mercury lamp, a shutter (Uniblitz), a filter wheel (Ludl Electronic Products), a dichroic mirror (460 nm), excitation (440 ± 10 nm) and emission (485 ± 15 nm for CFP and 530 ± 15 nm for YFP) filters (Cameleons 2 filter set 71007, Chroma Technologies, Rockingham, VT). A 40x 0.8 NA water immersion Fluor objective was used for simultaneous imaging and electrophysiology and a 10x 0.3 NA Plan Fluor objective for fluorescence imaging only. Fluorescence excitation was produced by two consecutive 200 to 500 ms long light pulses at 0.5 Hz and fluorescence emission was alternately collected at each wavelength with a back-illuminated, cooled CCD camera with the on-chip multiplication gain control (Cascade 512B, Photometrics). Image acquisition was controlled by RatioTool software (ISee Imaging Systems, Raleigh, NC) and a PowerMac G4 (Apple Computer).

Hippocampal slices were prepared, using conventional methods (Pettit and Augustine, 2000), from 2 to 3 week-old homozygous CLM1 mice. In brief, the brains were removed from

anesthetized and then decapitated animals and placed in a cold artificial cerebrospinal fluid (ACSF), containing (in mM): 125 NaCl, 2.5 KCl, 1.25 NaH_2PO_4, 26 $NaHCO_3$, 20 D(+)-glucose, 2 $CaCl_2$ and 1.3 $MgCl_2$, supplemented with 2–3 kynurenic acid (pH 7.4 after bubbling with 95 % O_2/5 % CO_2, v/v). A vibratome was used to make 250 μm thick coronal sections. The slices were then incubated at 36°C for 30 min prior to use.

The background-corrected intensity of YFP fluorescence was divided by that of CFP to calculate a ratio in each ROI that is inversely proportional to [Cl^-] (Fig. 4a). Autofluorescence accounted 1.5% or less of the total fluorescence and did not have any significance on the calculated ratio (Pond et al., 2006). For the images shown in the figures, raw images were smoothed by Gaussian filter (size: 20 μm) twice and then divided. Such ratio images were averaged over 4 repeated identical trials and then converted into [Cl^-]. Photobleaching of Clomeleon was minimized by attenuating the excitation light more than 500 fold by neutral density filters. The CCD camera was sometimes binned by the factor of 2 to increase the sensitivity. If any obvious trend due to photobleaching remained, it was corrected by fitting a regression line or an exponential to traces obtained without stimulus. All the image processing, analysis and statistical tests were done by IgorPro 5.0 (WaveMetrics, Lake Oswego, OR).

Procedures described in Pettit and Augustine (2000) were used to obtain whole-cell patch-clamp recordings from Clomeleon-positive CA1 pyramidal cells. Pipettes (5–6 MΩ) were filled with a solution that contained (in mM) 140 K-gluconate, 5 EGTA, 10 HEPES, 4 Na_2-ATP, 0.4 Na_3-GTP, 0.5 $CaCl_2$, 2 $MgCl_2$. pH and osmolarity were adjusted to 7.1 and 290 mmol/kg, respectively, with KOH. The cells were either voltage clamped at −50 to −40 mV to obtain outward Cl^- current or current clamped to obtain hyperpolarizing IPSP. Liquid junction potential was not corrected. When series resistance was 30 MΩ or more, dialysis of Clomeleon into the pipettes was negligible during the entire recording period of ~1 h.

A concentric bipolar metal electrode (diameter 125–250 μm) was placed at the boundary between stratum radiatum and lacunosum-moleculare to stimulate local inhibitory synapses on the apical dendrites of pyramidal cells. A train of electrical shocks of 100 to 200 μs in duration was delivered at 23 Hz with varying duration of 250 ms to 2 s by an isolated electrical stimulator (S44, Grass Instruments). Stimulation was repeated 3 to 4 times for signal averaging at the interval of 2 min after $[Cl^-]_i$ completely returned to the prestimulus level. The chamber was constantly superfused with oxygenated ACSF at 2 ml/min at room temperature (~23 °C). Kynurenic acid (2 to 3 mM) was routinely supplemented in ACSF to prevent excitatory glutamatergic transmission. SR95531 (Gabazine, 10 μM; Tocris, Ellisville, MI) was applied with the bath. In Ca^{2+}-free solution, $CaCl_2$ in ACSF was replaced by equimolar $MgCl_2$ and EGTA (2 mM) was added.

Calibration—The calibration constants R_{min} = 0.93, R_{max} = 2.40, and K_d' = 224 mM of equation (1) were determined *in situ* using solutions of F^-, gluconate and two known concentrations of Cl^- (50 and 134 mM) at pH 7.1. The F^- solution contained (in mM): 89 KF, 7 *N*-methyl-D-glucamine (NMDG), 7 HF, 1.25 NaH_2PO_4, 16 $KHCO_3$, 20 D(+)-glucose, 2 ethylene glycol-bis(2-aminoethylether)-*N*,*N*,*N*′,*N*′-tetraacetic acid (EGTA) and 5 NaOH. The gluconate solution contained (in mM): 45 NMDG, 45 D-gluconic acid, 92 K-gluconate, 1.25 NaH_2PO_4, 13 $KHCO_3$, 20 D(+)-glucose, 2 EGTA, 5 NaOH and 3.3 Mg-$gluconate_2$. The 134 mM Cl^- solution contained (in mM): 45 NMDG, 45 HCl, 1.25 NaH_2PO_4, 15 $KHCO_3$, 20 D (+)-glucose, 2 EGTA, 5 NaOH and 3.3 Mg-$gluconate_2$. The 50 mM Cl^- solution was obtained by mixing appropriate proportions of gluconate and 134 mM Cl^- solutions. The Cl^-/OH^- antiporter tributyltin acetate (20 μM) and the K^+/H^+ ionophore nigericin (20 μM) were first dissolved in ethanol and then diluted into solutions to remove the Cl^- and H^+/OH^- gradients, respectively.

Acknowledgements

We thank R. L. Dunbar for participating in initial experiments, W. Drake, E. Ellison, and T. Schweizer for technical assistance, W. Denk for providing access to a spinning disk confocal microscope, G. Giese for help with confocal microscopy, B. Sakmann and P. Seeburg for generous support, F. Galeffi, K. Tanaka and R. Yasuda for their comments on this manuscript and A. Frick for advice on preparation of hippocampal slices. K.B. was a Research Fellow of the Japan Society for the Promotion of Science. This work was partially supported by DFG grant KU1983/1-2 (FOR 577) awarded to T.K., NIH grants awarded to G.J.A. and G.F., as well as an Alfred P. Sloan Research Fellowship, a Klingenstein Fellowship Award in the Neuroscience and a Beckman Young Investigator Award to G.F.

References

Agmon A, Connors BW. Correlation between intrinsic firing patterns and thalamocortical synaptic responses of neurons in mouse barrel cortex. J Neurosci 1992;12:319–329. [PubMed: 1729440]

Alger BE, Nicoll RA. GABA-mediated biphasic inhibitory responses in hippocampus. Nature 1979;281:315–317. [PubMed: 551280]

Andersen P, Dingledine R, Gjerstad L, Langmoen IA, Laursen AM. Two different responses of hippocampal pyramidal cells to application of gamma-amino butyric acid. J Physiol (Lond) 1980;305:279–296. [PubMed: 7441554]

Baker BJ, Kosmidis EK, Vucinic D, Falk CX, Cohen LB, Djurisic M, Zecevic D. Imaging brain activity with voltage- and calcium-sensitive dyes. Cell Mol Neurobiol 2005;25:245–282. [PubMed: 16050036]

Barker JL, Ransom BR. Amino acid pharmacology of mammalian central neurones grown in tissue culture. J Physiol (Lond) 1978;280:331–354. [PubMed: 690884]

Ben-Ari Y, Cherubini E, Corradetti R, Gaiarsa JL. Giant synaptic potentials in immature rat CA3 hippocampal neurones. J Physiol (Lond) 1989;416:303–325. [PubMed: 2575165]

Berglund, K.; Dunbar, RL.; Lee, P.; Feng, G.; Augustine, GJ. A practical guide: Imaging synaptic inhibition with Clomeleon, a genetically encoded chloride indicator. In: Konnerth, A.; Yuste, R., editors. Imaging in Neuroscience and Development: A Laboratory Manual. Cold Spring Harbor: Cold Spring Harbor Laboratory Press; 2005. p. 595-598.

Bevensee MO, Cummins TR, Haddad GG, Boron WF, Boyarsky G. pH regulation in single CA1 neurons acutely isolated from the hippocampi of immature and mature rats. J Physiol (Lond) 1996;494:315–328. [PubMed: 8841993]

Caroni P. Overexpression of growth-associated proteins in the neurons of adult transgenic mice. J Neurosci Methods 1997;71:3–9. [PubMed: 9125370]

Cherubini E, Gaiarsa JL, Ben-Ari Y. GABA: an excitatory transmitter in early postnatal life. Trends Neurosci 1991;14:515–519. [PubMed: 1726341]

Cohen D, Yarom Y. Cerebellar on-beam and lateral inhibition: two functionally distinct circuits. J Neurophysiol 2000;83:1932–1940. [PubMed: 10758104]

Derdikman D, Hildesheim R, Ahissar E, Arieli A, Grinvald A. Imaging spatiotemporal dynamics of surround inhibition in the barrels somatosensory cortex. J Neurosci 2003;23:3100–3105. [PubMed: 12716915]

Duarte CB, Ferreira IL, Carvalho AP, Carvalho CM. Relation of exocytotic release of γ-aminobutyric acid to Ca^{2+} entry through Ca^{2+} channels or by reversal of the Na^{+}/Ca^{2+} exchanger in synaptosomes. Pflügers Archiv - European Journal of Physiology 1993;423:314–323.

Duebel J, Haverkamp S, Schleich W, Feng G, Augustine GJ, Kuner T, Euler T. Two-photon imaging reveals somatodendritic chloride gradient in retinal ON-type bipolar cells expressing the biosensor Clomeleon. Neuron 2006;49:81–94. [PubMed: 16387641]

Ebner TJ, Chen G, Gao W, Reinert K. Optical imaging of cerebellar functional architectures: parallel fiber beams, parasagittal bands and spreading acidification. Prog Brain Res 2005;148:125–138. [PubMed: 15661186]

Elias SA, Yae H, Ebner TJ. Optical imaging of parallel fiber activation in the rat cerebellar cortex: spatial effects of excitatory amino acids. Neuroscience 1993;52:771–786. [PubMed: 8095709]

Feng G, Lu J, Gross J. Generation of transgenic mice. Methods in Molecular Medicine 2004;99:255–267. [PubMed: 15131343]

Feng G, Mellor RH, Bernstein M, Keller-Peck C, Nguyen QT, Wallace M, Nerbonne JM, Lichtman JW, Sanes JR. Imaging neuronal subsets in transgenic mice expressing multiple spectral variants of GFP. Neuron 2000;28:41–51. [PubMed: 11086982]

Freund TF, Buzsáki G. Interneurons of the hippocampus. Hippocampus 1996;6:347–470. [PubMed: 8915675]

Grinvald A, Hildesheim R. VSDI: a new era in functional imaging of cortical dynamics. Nature Reviews Neuroscience 2004;5:874–885.

Hasan MT, Friedrich RW, Euler T, Larkum ME, Giese G, Both M, Duebel J, Waters J, Bujard H, Griesbeck O, et al. Functional fluorescent Ca^{2+} indicator proteins in transgenic mice under TET control. PLoS Biology 2004;2:e163. [PubMed: 15208716]

Haverkamp S, Wassle H, Duebel J, Kuner T, Augustine GJ, Feng G, Euler T. The primordial, blue-cone color system of the mouse retina. J Neurosci 2005;25:5438–5445. [PubMed: 15930394]

Horikawa J, Hosokawa Y, Kubota M, Nasu M, Taniguchi I. Optical imaging of spatiotemporal patterns of glutamatergic excitation and GABAergic inhibition in the guinea-pig auditory cortex *in vivo*. J Physiol (Lond) 1996;497:629–638. [PubMed: 9003549]

Huguenard JR, Alger BE. Whole-cell voltage-clamp study of the fading of GABA-activated currents in acutely dissociated hippocampal neurons. J Neurophysiol 1986;56:1–18. [PubMed: 3746390]

Inglefield JR, Schwartz-Bloom RD. Confocal imaging of intracellular chloride in living brain slices: measurement of $GABA_A$ receptor activity. J Neurosci Methods 1997;75:127–135. [PubMed: 9288644]

Isomura Y, Sugimoto M, Fujiwara-Tsukamoto Y, Yamamoto-Muraki S, Yamada J, Fukuda A. Synaptically activated Cl^- accumulation responsible for depolarizing GABAergic responses in mature hippocampal neurons. J Neurophysiol 2003;90:2752–2756. [PubMed: 14534278]

Jedlička P, Backus KH. Inhibitory transmission, activity-dependent ionic changes and neuronal network oscillations. Physiol Res 2006;55:139–149. [PubMed: 15910171]

Kaila K. Ionic basis of $GABA_A$ receptor channel function in the nervous system. Prog Neurobiol 1994;42:489–537. [PubMed: 7522334]

Kuner T, Augustine GJ. A genetically encoded ratiometric indicator for chloride: capturing chloride transients in cultured hippocampal neurons. Neuron 2000;27:447–459. [PubMed: 11055428]

Maccaferri G, Roberts JD, Szucs P, Cottingham CA, Somogyi P. Cell surface domain specific postsynaptic currents evoked by identified GABAergic neurones in rat hippocampus *in vitro*. J Physiol (Lond) 2000;524:91–116. [PubMed: 10747186]

Mao BQ, Hamzei-Sichani F, Aronov D, Froemke RC, Yuste R. Dynamics of spontaneous activity in neocortical slices. Neuron 2001;32:883–898. [PubMed: 11738033]

Marandi N, Konnerth A, Garaschuk O. Two-photon chloride imaging in neurons of brain slices. Pflügers Archiv - European Journal of Physiology 2002;445:357–365.

Mody I, Pearce RA. Diversity of inhibitory neurotransmission through $GABA_A$ receptors. Trends Neurosci 2004;27:569–575. [PubMed: 15331240]

Mrsic-Flogel T, Hübener M, Bonhoeffer T. Brain mapping: new wave optical imaging. Curr Biol 2003;13:R778–780. [PubMed: 14521859]

Obata K, Oide M, Tanaka H. Excitatory and inhibitory actions of GABA and glycine on embryonic chick spinal neurons in culture. Brain Res 1978;144:179–184. [PubMed: 638760]

Owens DF, Boyce LH, Davis MB, Kriegstein AR. Excitatory GABA responses in embryonic and neonatal cortical slices demonstrated by gramicidin perforated-patch recordings and calcium imaging. J Neurosci 1996;16:6414–6423. [PubMed: 8815920]

Payne JA, Rivera C, Voipio J, Kaila K. Cation-chloride co-transporters in neuronal communication, development and trauma. Trends Neurosci 2003;26:199–206. [PubMed: 12689771]

Pérez-Garci E, Gassmann M, Bettler B, Larkum ME. The $GABA_{B1b}$ isoform mediates long-lasting inhibition of dendritic Ca^{2+} spikes in layer 5 somatosensory pyramidal neurons. Neuron 2006;50:603–616. [PubMed: 16701210]

Perkins KL, Wong RK. The depolarizing GABA response. Can J Physiol Pharmacol 1997;75:516–519. [PubMed: 9250386]

Pettit DL, Augustine GJ. Distribution of functional glutamate and GABA receptors on hippocampal pyramidal cells and interneurons. J Neurophysiol 2000;84:28–38. [PubMed: 10899180]

Pond BB, Berglund K, Kuner T, Feng G, Augustine GJ, Schwartz-Bloom RD. The chloride transporter Na^+-K^+-Cl^- cotransporter isoform-1 contributes to intracellular chloride increases after *in vitro* ischemia. J Neurosci 2006;26:1396–1406. [PubMed: 16452663]

Reiff DF, Ihring A, Guerrero G, Isacoff EY, Joesch M, Nakai J, Borst A. *In vivo* performance of genetically encoded indicators of neural activity in flies. J Neurosci 2005;25:4766–4778. [PubMed: 15888652]

Reuter D, Zierold K, Schröder WH, Frings S. A depolarizing chloride current contributes to chemoelectrical transduction in olfactory sensory neurons *in situ*. J Neurosci 1998;18:6623–6630. [PubMed: 9712634]

Rivera C, Voipio J, Kaila K. Two developmental switches in GABAergic signalling: the K^+-Cl^- cotransporter KCC2 and carbonic anhydrase CAVII. J Physiol (Lond) 2005;562:27–36. [PubMed: 15528236]

Rivera C, Voipio J, Payne JA, Ruusuvuori E, Lahtinen H, Lamsa K, Pirvola U, Saarma M, Kaila K. The K^+/Cl^- co-transporter KCC2 renders GABA hyperpolarizing during neuronal maturation. Nature 1999;397:251–255. [PubMed: 9930699]

Somogyi P, Klausberger T. Defined types of cortical interneurone structure space and spike timing in the hippocampus. J Physiol (Lond) 2005;562:9–26. [PubMed: 15539390]

Staley KJ, Proctor WR. Modulation of mammalian dendritic $GABA_A$ receptor function by the kinetics of Cl^- and HCO^{3-} transport. J Physiol (Lond) 1999;519:693–712. [PubMed: 10457084]

Stein V, Hermans-Borgmeyer I, Jentsch TJ, Hübner CA. Expression of the KCl cotransporter KCC2 parallels neuronal maturation and the emergence of low intracellular chloride. J Comp Neurol 2004;468:57–64. [PubMed: 14648690]

Szabadics J, Varga C, Molnár G, Oláh S, Barzó P, Tamás G. Excitatory effect of GABAergic axo-axonic cells in cortical microcircuits. Science 2006;311:233–235. [PubMed: 16410524]

Thompson SM, Gähwiler BH. Activity-dependent disinhibition. I Repetitive stimulation reduces IPSP driving force and conductance in the hippocampus in vitro. J Neurophysiol 1989;61:501–511. [PubMed: 2709096]

Verkman AS. Development and biological applications of chloride-sensitive fluorescent indicators. Am J Physiol 1990;259:C375–388. [PubMed: 2205105]

Wimmer VC, Nevian T, Kuner T. Targeted in vivo expression of proteins in the calyx of Held. Pflügers Archiv - European Journal of Physiology 2004;449:319–333.

Yamada J, Okabe A, Toyoda H, Kilb W, Luhmann HJ, Fukuda A. Cl^- uptake promoting depolarizing GABA actions in immature rat neocortical neurones is mediated by NKCC1. J Physiol (Lond) 2004;557:829–841. [PubMed: 15090604]

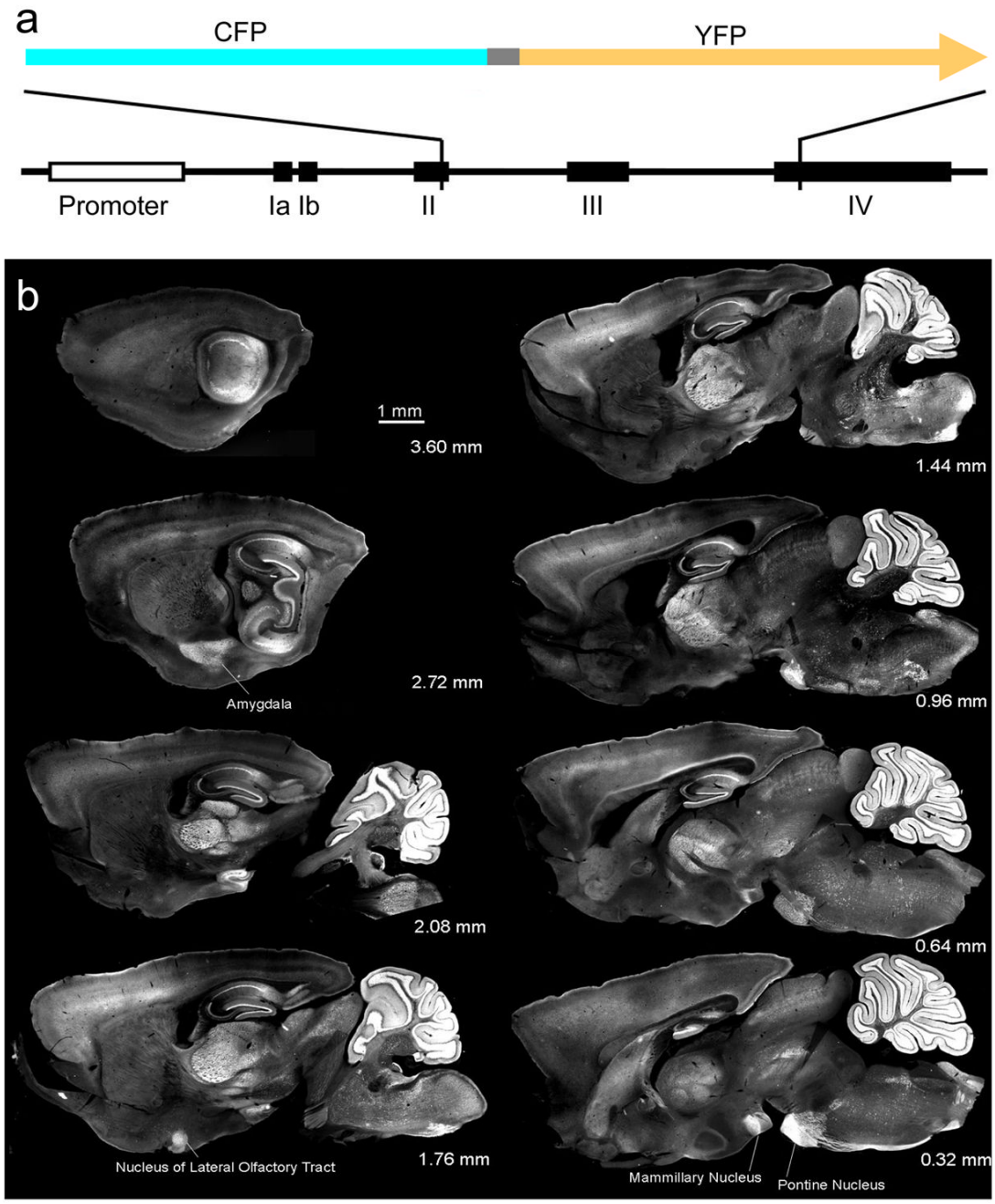

Fig. 1. Clomeleon expression in the brain of transgenic mice

(a) The cDNA of Clomeleon: Cyan fluorescent protein (CFP), a linker of 24 amino acid residues (grey), and the yellow fluorescent protein (YFP) Topaz. Partial schematic structure of the *thy1* gene with exons labeled in roman numerals.

(b) Series of sagittal brain sections of an adult CLM1 mouse. Distance from midline is indicated in each panel. YFP fluorescence was recorded with a 2x objective lens.

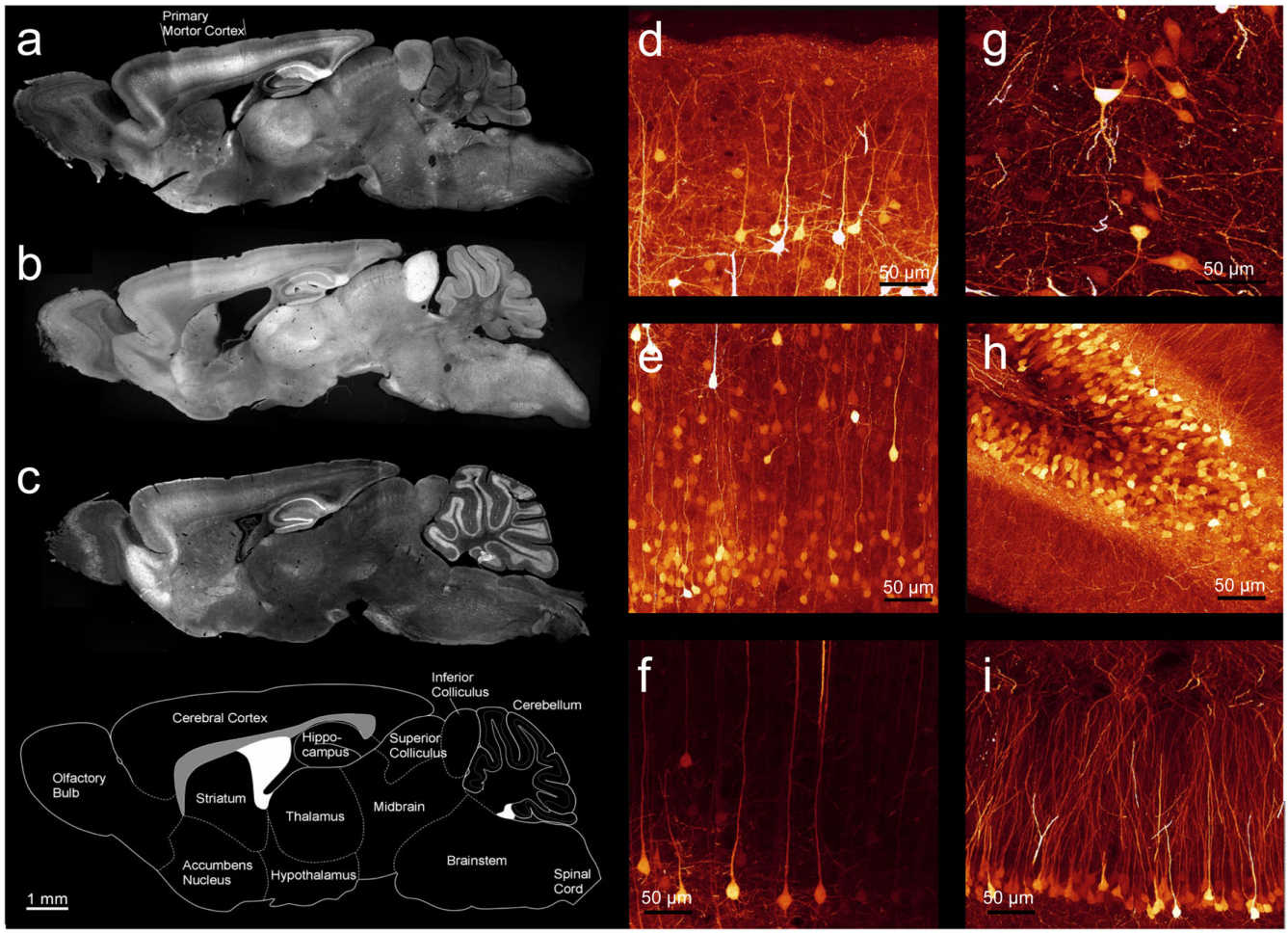

Fig. 2. Differential expression of Clomeleon in CLM lines

(a–c) YFP fluorescence images of paramedial sagittal sections of fixed brains of adult mice from lines CLM11, 12 and 13. (d–i) Confocal images of sections taken from CLM-11, shown as maximal projections of an image stack: layer 2/3 (d) and layer 5 of two different regions (e, f) of the cortex; hilus (g), dentate gyrus (h), and CA1 neurons (i) of the hippocampus.

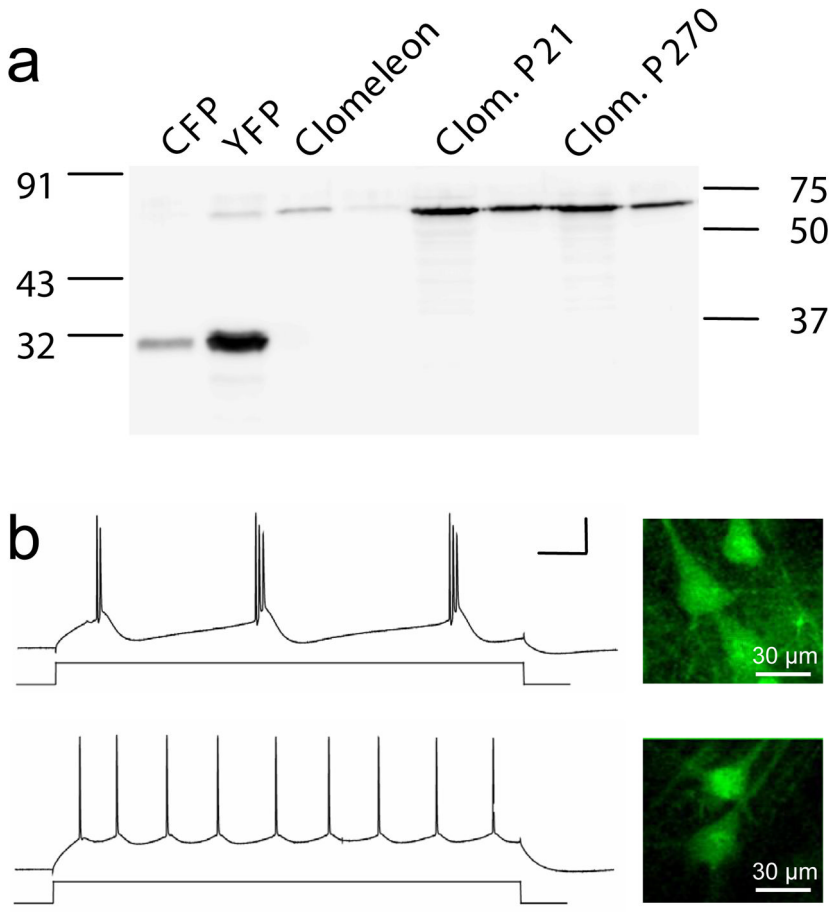

Fig. 3. Long-term effects and functionality of Clomeleon overexpression in mice

(a) Western blot showing recombinant and in vivo expressed Clomeleon protein. Two different amounts of brain lysates were loaded.

(b) Cortical layer 5 neurons recorded with two-photon laser-scanning microscope in acute slices obtained from P14 CLM11 mice. Insets show neurons from which recordings were obtained. Scale bar: 100 ms (horizontal), 50 mV (vertical).

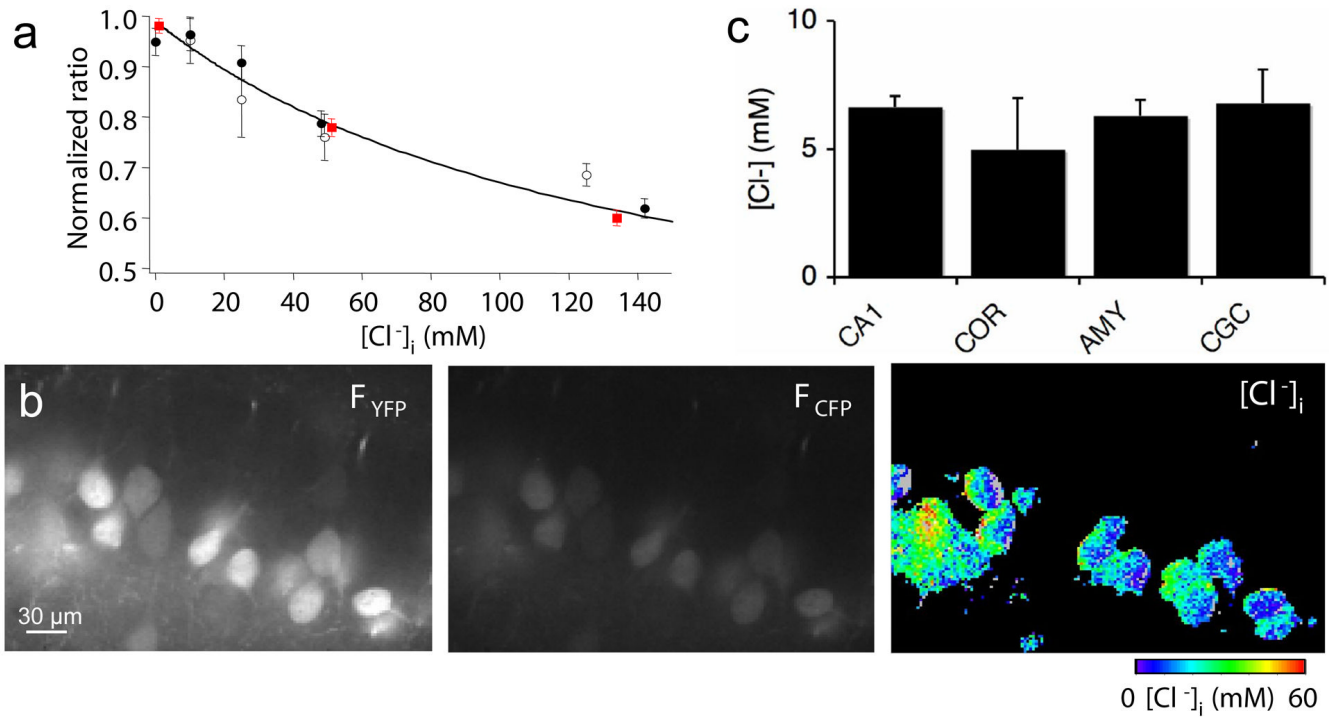

Fig. 4. Measuring resting $[Cl^-]_i$ in neurons

(a) Calibration in cultured hippocampal neurons via the patch pipette (open circles, n = 4–12 experiments for each concentration) and the nigericin-tributyltin method (filled circles, n = 29–46) compared with calibrations done in slices with the nigericin-tributyltin method (filled red squares, n = 24–37). Ratios were normalized to R_{max} at 0 $[Cl^-]$ to allow comparison of data obtained on different imaging systems. A fit of equation (1) to the average of the data points yielded $K_d' = 142$ mM. Data points at 50 mM were displaced horizontally to improve visibility.

(b) Spinning-disk confocal microscope imaging of YFP (left) and CFP (center) fluorescence of CA1 neurons in hippocampal slice from P21 mouse. Ratio of these fluorescence signals yielded the pseudocolor map of $[Cl^-]_i$ at right.

(c) Somatic resting $[Cl^-]_i$ in hippocampal CA1 neurons (CA1), pyramidal cells of cortex (COR), principal neurons of the amygdala (AMY), and cerebellar granule cells (CGC). Values indicate mean ± SEM (n = 13–69).

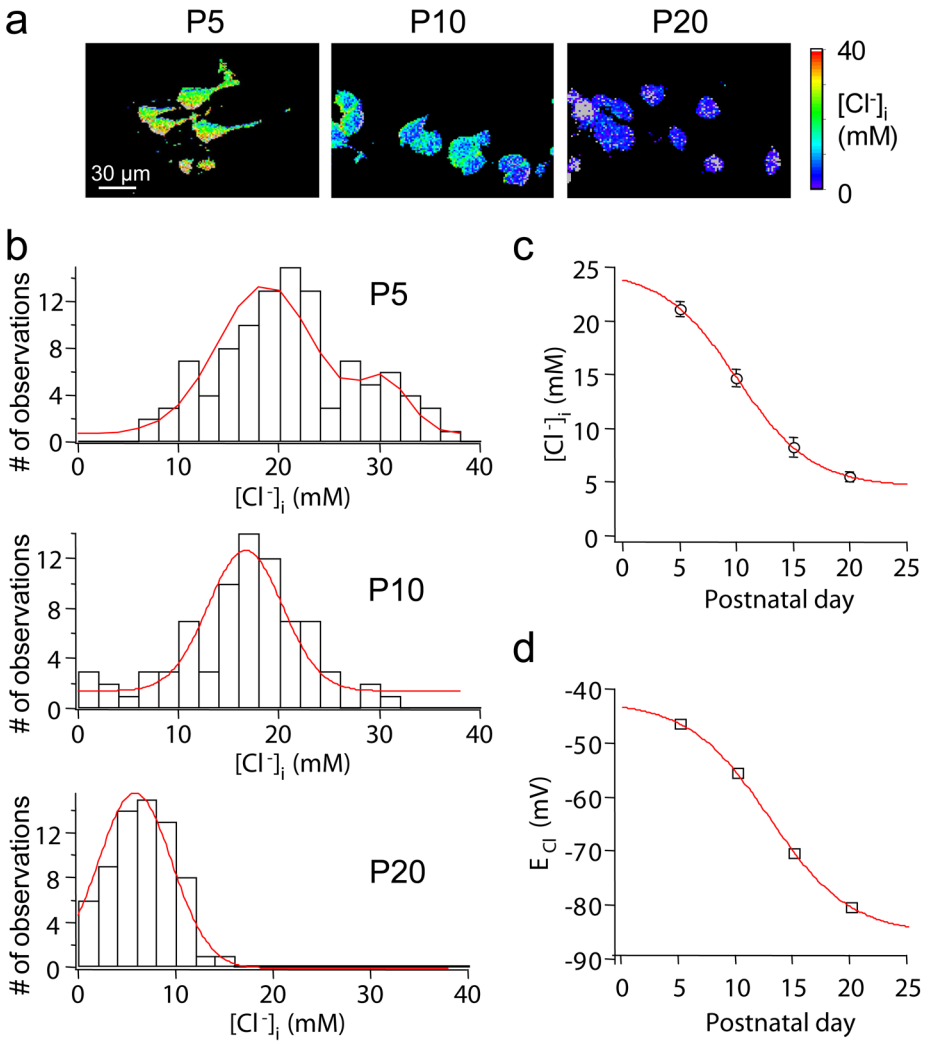

Fig. 5. Developmental changes in $[Cl^{-}]_I$

(a) Pseudo-color images showing $[Cl^{-}]_i$ at different postnatal stages. Images were obtained with a confocal microscope and clipped to the same intensity range.

(b) Distribution of resting $[Cl^{-}]_i$ at P5, P10 and P20. Gauss fits yielded (mean ± width) 18.6 ± 6.8 and 30.4 ± 3.7 mM at P5, 16.6 ± 5.2 at P10, 5.8 ± 5.4 at P20.

(c) Summary of the data shown in b. Mean $[Cl^{-}]_i$ (open circles) could be described with a sigmoidal function (error bars indicate SEM).

(d) E_{Cl} calculated from the Nernst equation (E_{Cl} = 58 mV * log($[Cl^{-}]_i$/134 mM).

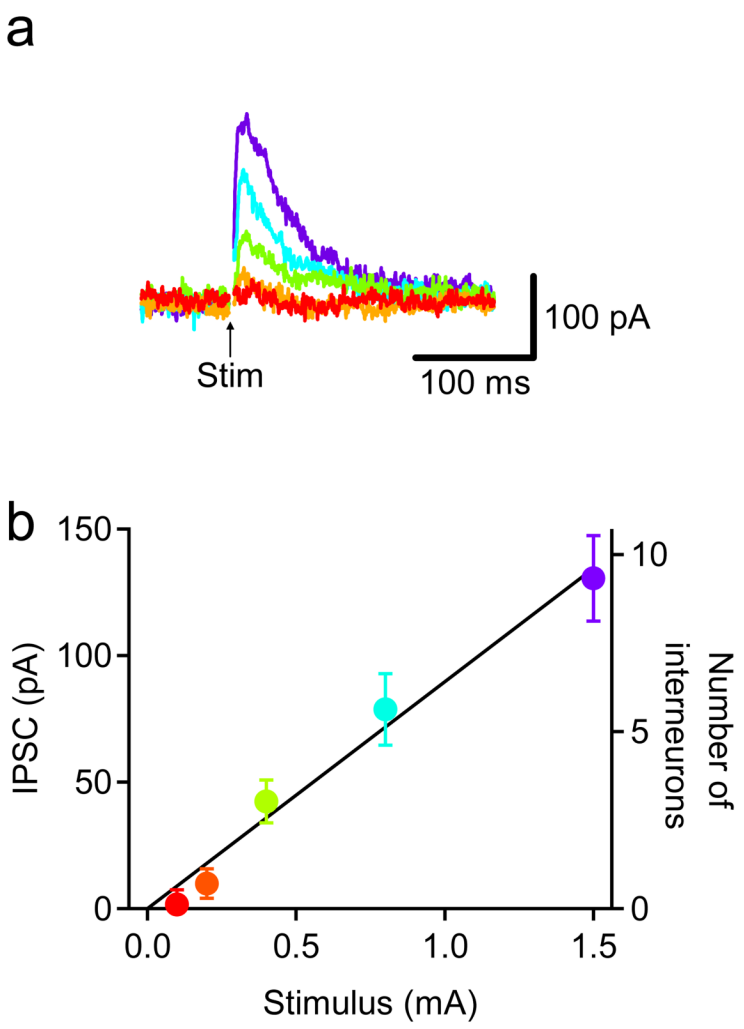

Fig. 6. IPSCs to various intensity of single stimuli

(a) Representative IPSCs recorded from a CA1 pyramidal cell to single stimuli (Stim) of various intensity. The intensity of stimuli is indicated by the colors of traces that match those in b.

(b) Dependence of IPSCs on the intensity of stimuli. Peak IPSCs were converted into the number of interneurons according to Maccaferri et al. (2000). Mean ± SEM of 7 experiments.

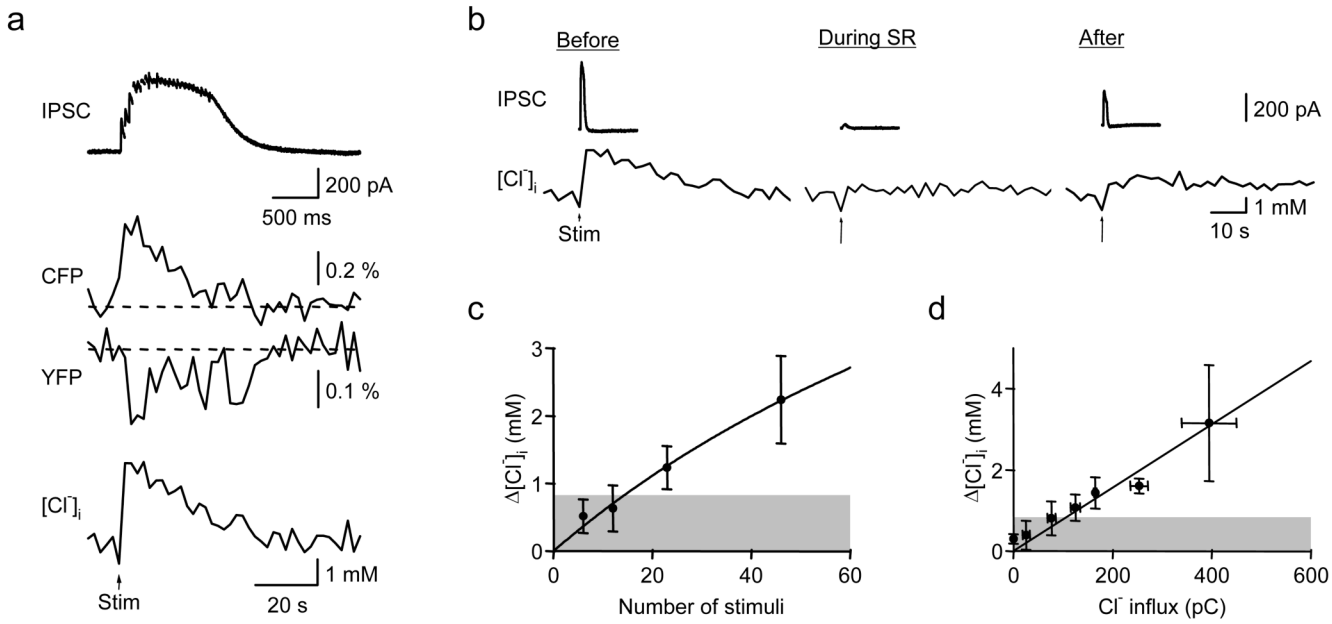

Fig. 7. Simultaneous recordings of IPSCs and $[Cl^-]_i$ during synaptic stimulation

(a) Current (upper trace), simultaneous fluorescence ($\Delta F/F_0$, center traces) and Cl^- signals (bottom trace) from the soma of a CLM1 hippocampal CA1 pyramidal cell (P20). Each trace represents an average of 3 individual responses. IPSCs are shown on an expanded time scale to allow resolution of individual responses. Stimulus artifacts were blanked for clarity. The arrows (Stim) in a and b depict the time of electrical stimulation (1 s, 23 Hz) at the border of stratum radiatum and lacunosum-moleculare. Fluorescence imaging in this and all subsequent figures was done with a wide-field microscope.

(b) Both IPSC and Cl^- transient (left) were blocked by SR (center) and partially recovered after washout (right). SR was applied at 10 μM.

(c) Correlation of changes in $[Cl^-]_i$ and the numbers of stimuli in trains. Each point and error bar represents average and SEM, respectively, from 6 cells. A shaded region denotes RMS value of basal fluctuation in $[Cl^-]_i$ in single trials.

(d) Correlation of changes in $[Cl^-]_i$ and Cl^- influx. 3–11 responses from 14 cells were binned.

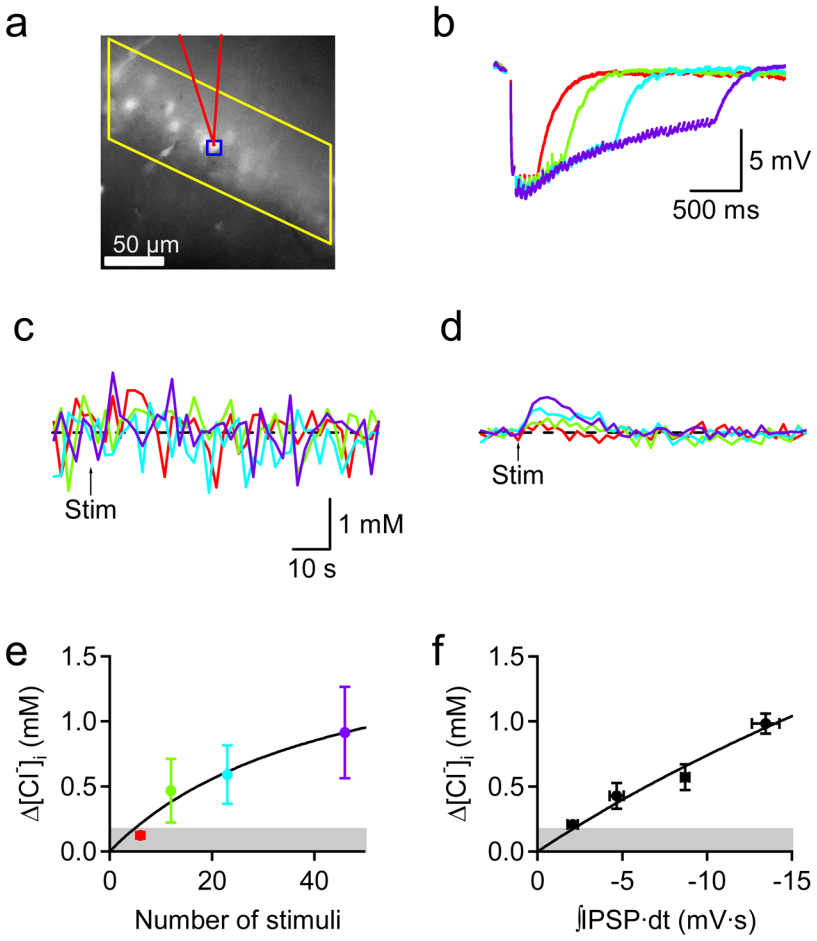

Fig. 8. Simultaneous recordings of IPSPs and $[Cl^-]_i$ during synaptic stimulation

(a) YFP fluorescence in hippocampal CA1 neurons of an acute brain slice obtained from a CLM1 mouse at P17. A whole-cell recording was established from the pyramidal neuron at the tip of the patch pipette (shown in red). $[Cl^-]_i$ was recorded from the soma of the recorded neuron (indicated by blue square) and surrounding pyramidal neurons (area indicated by yellow parallelogram).

(b) Somatic membrane potential recording from the cell shown in a. Responses produced by four different trains of stimuli are indicated by the same color in panels a to e (see e for the number of stimuli in each train). Traces represent average of 4 trials.

(c) Somatic $[Cl^-]_i$ recording of the cell shown in a and b; trace represents average of 4 trials. Arrow (Stim) indicates time of electrical stimulation. (d) Recording of average changes in $[Cl^-]_i$ recorded from the yellow area shown in **a**. Arrow (Stim) indicates time of electrical stimulation and traces represent average of 4 trials. The calibration bar in c also applies to d.

(e) Correlation between changes in average $[Cl^-]_i$ and the number of stimuli. Each point and error bar represents average and SEM, respectively, from 4 slices. Shaded region denotes RMS value of basal fluctuations in $[Cl^-]_i$ recorded from the stratum pyramidale without averaging over trials.

(f) Correlation between changes in $[Cl^-]_i$ and time integrals of IPSPs. 2–16 responses from 4 cells were binned.

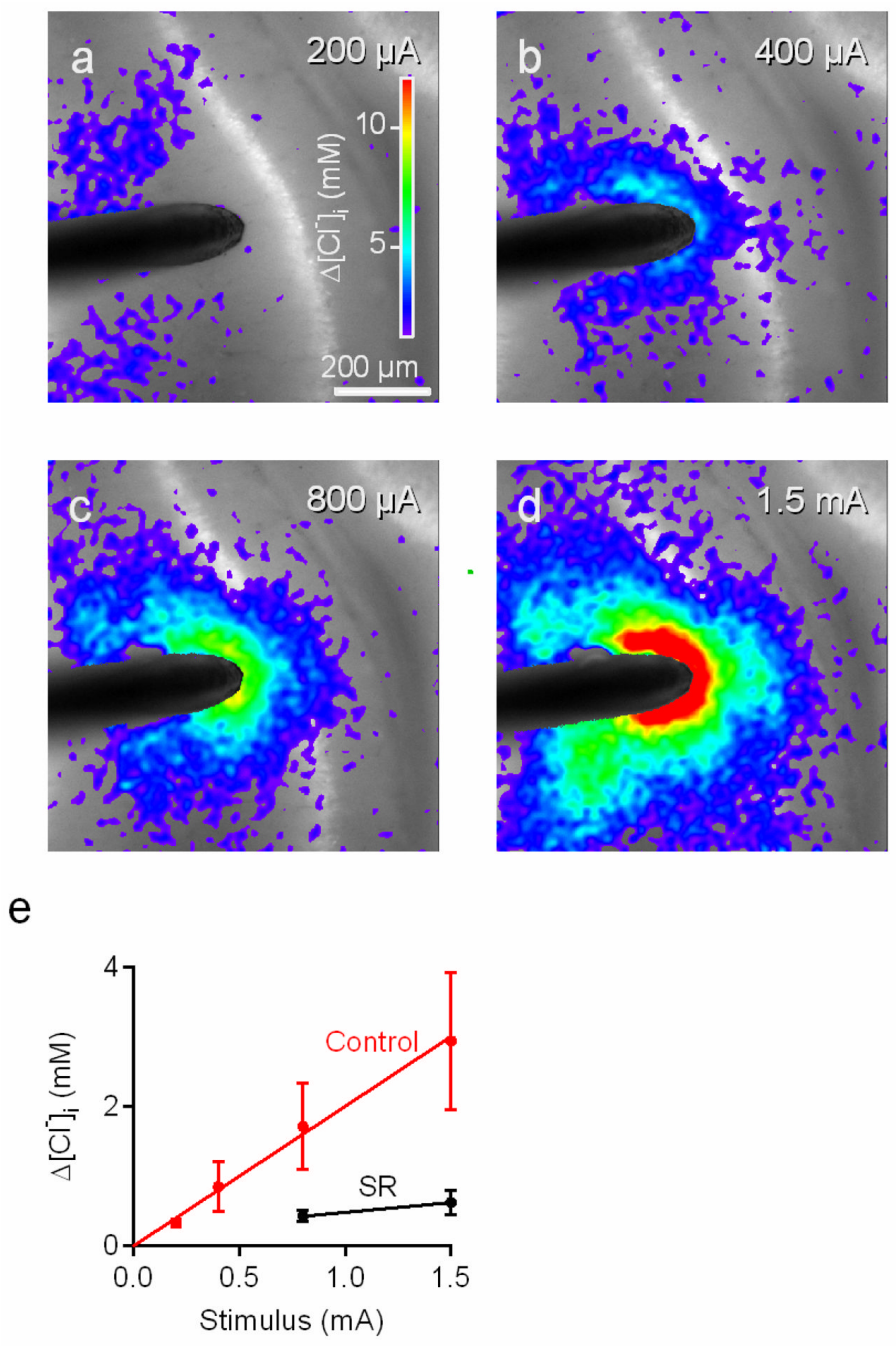

Fig. 9. Cl^- responses to varying stimulus intensity

(a–d) Images showing Cl^- changes (pseudo-color scale) superimposed on YFP fluorescence image (grey scale) measured in CLM1 hippocampal slice (P21). Electrical stimulation was delivered for 1 s with a current of 200 µA (a), 400 µA (b), 800 µA (c), or 1.5 mA (d). Images were acquired 4 s after each stimulus.

(e) Dependence of $[Cl^-]_i$ changes, measured from whole CA1 field, on the intensity of stimuli before (Control) and during application of 10-µM SR (SR). The response was fitted with a linear regression that went through the origin with a slope of 2.0 mM/mA. Mean ± SEM of 4 experiments.

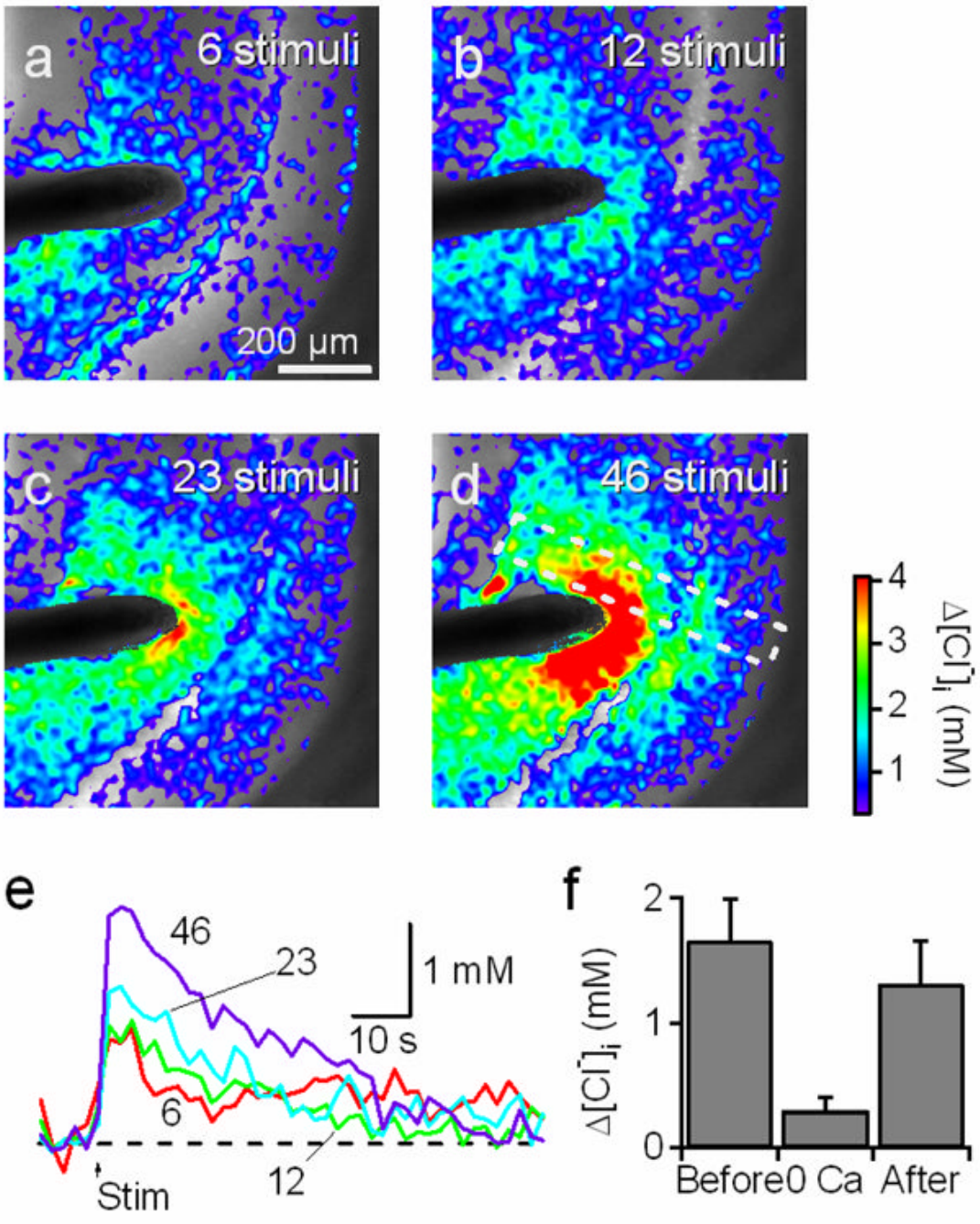

Fig. 10. Cl^- transients elicited by synaptic stimulation in unperturbed neurons

(a–d) Images showing Cl^- changes (pseudo-color) superimposed on YFP fluorescence (grey scale) measured in CLM1 hippocampal slice (P16). The slice was oriented so that the stratum lacunosum-moleculare/radiatum (apical dendrites) to the left, the stratum pyramidale (somata) at center, and the stratum oriens (basal dendrites) to the right. A train of brief electrical stimuli (800 µA; 23 Hz) was delivered by the electrode (black) for 250 ms (6 stimuli, a), for 500 ms (12 stimuli, b), for 1 s (23 stimuli, c) and 2 s (46 stimuli, d). Cl^- was imaged every 2 s and repeated 4 times for each duration for averaging. The region within the white dotted rectangle was used for further analysis in Fig. 11.

(e) Changes in $[Cl^-]_i$ averaged over the whole CA1 in the field shown in a-d. The arrow (Stim) depicts the onset of electrical stimulation.
(f) Reversible decrease of Cl^- response in nominally Ca^{2+}-free solution. The duration of the train was 1 s (23 stimuli). Mean ± SEM of 6 experiments.

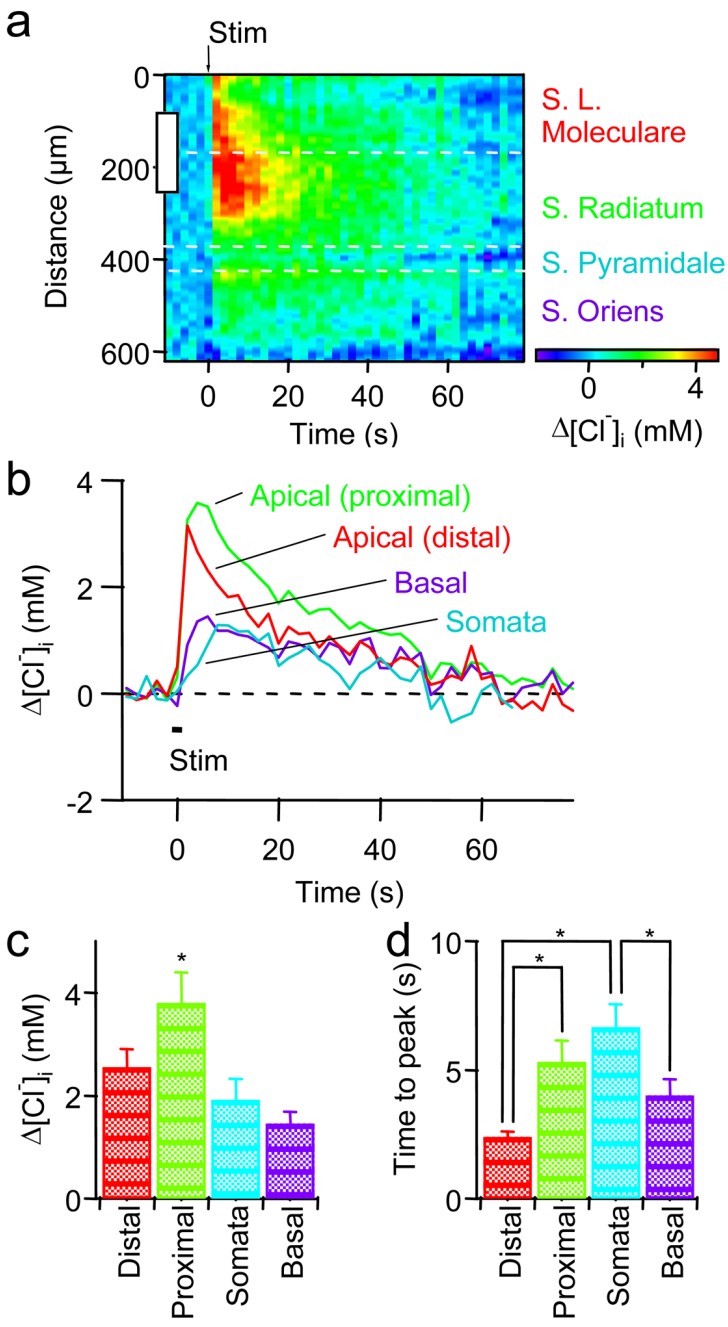

Fig. 11. Spatiotemporal profiles of Cl^- transients

(a) A line-scan of $[Cl^-]_i$ changes across the layers of CA1. The area of analysis is indicated by the white dotted rectangle in Fig. 10d and resting $[Cl^-]_i$ before stimuli was subtracted to show relative changes caused by stimulation (at arrow). A white rectangle on the ordinate denotes the size and the position of the stimulating electrode.

(b) Changes in $[Cl^-]_i$ calculated from each layer. Trace colors correspond to those of labels in a. Duration of 2 s stimulus train is depicted as a line (Stim).

(c) Peak magnitude of $[Cl^-]_i$ changes in the four compartments of pyramidal cells in each layer. Mean ± SEM of 7 experiments. * denotes a significant difference from the rest by ANOVA followed by Newman-Keuls test (*$p < 0.05$).

(d) Time to peak of $[Cl^-]_i$ changes in the same four compartments of pyramidal cells. * denotes a significant difference, as determined by ANOVA followed by Newman-Keuls test (*$p < 0.05$).

Table 1

Expression patterns in Clomeleon mouse lines

CLM	1	2	9	11	12	13
Olfactory bulb						
Glomeruli	++	++	++	−	+	+
External plexiform layer	+	−	+	−	+	−
Mitral cells	+++	++	−	+	++	−
Internal plexiform layer	+	−	+	++	+	−
Neocortex						
Layer 1	+	−	−	+	−	−
Layer 2/3	++	−	−	+	+	++
Layer 4	+	−	−	−	−	+
Layer 5	+++	−	−	+++	++	+
Layer 6	++	−	−	++	++	+
Hippocampus						
DG	+++	++	++	++	+	+++
Hilus	+	−	−	++	+	+
CA3	+	+	++	+	−	++
CA2	+	+++	++	+	−	++
CA1	+++	++	+++	+++	++	+++
Stratum lucidum	−	+	−	−	+	+
Basal ganglia	+	+	++	+	+	+
Amygdala	+++	−	−	+++	++	+++
Thalamus	++	+	+	++	+++	++
Cerebellum						
Mossy fibers	−	++	++	+++	++	+++
Granule cells	+++	−	−	−	−	−
Purkinje cells	−	−	−	+	−	−
Nuclei	−		−	+++	+++	+++
Brainstem	++	+	++	++	++	++
Spinal cord						
α-Motoneurons	+			++		
Dorsal horn	+			+		

CLM	1	2	9	11	12	13
Retina						
Bipolar cells	+++	+	–	++	+	–
Amacrine cells	+	+	++	+	++	–
Ganglion cells	+++	+	+++	++	–	++

“+++”, “++”, “+” denote high, medium and low density, respectively, of Clomeleon-expressing neurons within each area. “–” denotes no expression.

Table 2

Electrophysiological properties of cortical layer 5 Clomeleon-expressing and wildtype neurons

	CLM		Wildtype	
Property	**Regular spiking**	**Bursting**	**Regular spiking**	**Bursting**
Number of neurons examined	30	41	8	6
Resting membrane potential (RMP, mV)	−66 ± 6	−68 ± 5	−64 ± 5	−63 ± 3
Input resistance (MΩ)	64 ± 24	63 ± 22	54 ± 14	58 ± 13
Action potential (AP) amplitude (RMP to peak, mV)	95 ± 16	98 ± 14	94 ± 11	94 ± 6
AP threshold (mV)	−45 ± 6	−45 ± 4	−41 ± 5	−40 ± 6

All numbers reflect mean ± SD.